**Applied Science, Computing and Energy, 2026, 4(1), 122-154**

# Comparative Assessment of Granite-Hosted Pegmatite- Quartz Veins in Akpet and Betem as a Potential for High-purity Quartz Resource

**Benjamin Odey Omang [*], Godwin Terwase Kave, Henry Francis Effiom, Andrew Kalu Njoku, Josephine Uzibe Odey,**

**01 January 2025/Accepted: 16 February 2026 /Published: 20 February 2026**

***Abstract:*** *This study presents a comparative geological and geochemical assessment of granite-hosted pegmatite-quartz veins in Akpet and Betem areas, southeastern Nigeria, to evaluate their potential as sources of high-purity quartz (HPQ). A total of thirty (30) samples were subjected to mineralogical (using photomicrographs), geochemical (using Scanning Electron Microscopy and Energy Dispersive X-ray Spectroscopy – SEM and EDS), and statistical analyses (One-Way ANOVA and Principal Component Analysis) to determine the genesis, impurity levels, and economic viability of quartz in both regions. The results reveal distinct genetic environments for the two sites: Akpet quartz veins are associated with orogenic processes, formed under high-pressure and moderate-temperature conditions during the Pan-African orogeny, while Betem quartz is linked to epithermal systems, formed at lower pressures and temperatures in a shallow magmatic-hydrothermal environment. Trace element geochemistry indicates significantly lower concentrations of impurities such as Al, Ti, Li, and Fe in Akpet quartz compared to Betem. These elements are critical in determining quartz suitability for high-tech applications. Principal component analysis highlights that Akpet quartz is relatively purer and less mineral-inclusion-rich, with better potential for beneficiation to meet HPQ specifications. In contrast, Betem quartz exhibits high concentrations of contaminant trace elements and mineral inclusions (e.g., zircon, monazite, titanite), suggesting a more evolved pegmatitic system with lower potential for economic HPQ extraction without extensive processing. The study concludes that Akpet quartz, while not naturally meeting HPQ standards, holds promise for semi-industrial applications and can be upgraded using cost-effective beneficiation techniques such as acid or alkaline leaching, given its relatively low impurity levels and favorable geochemical characteristics. Conversely, the high impurity burden in Betem quartz makes it more suitable for low-grade industrial or construction uses unless advanced purification technologies are employed. These findings provide valuable insights for targeted HPQ exploration and resource development in Nigeria's Basement Complex.*

***Keywords:*** *Akpet, Betem, High-Purity Quartz (HPQ), Scanning Electron Microscopy and Energy Dispersive X-ray Spectroscopy – SEM and EDS Pan-African Orogeny, Epithermal Systems.*

**Benjamin Odey Omang**
Department of Geology, University of Calabar, P.M.B 1115, Calabar, Cross River State, Nigeria
**Email:** odeyben@gmail.com
**https://orcid.org/0000-0001-9196-3109**

**Godwin Terwase Kave**
Department of Geology, University of Calabar, P.M.B 1115, Calabar, Cross River State, Nigeria
**Email:** gkaves@yahoo.com

**Henry Francis Effiom**
Department of Geology, University of Calabar, P.M.B 1115, Calabar, Cross River State, Nigeria
**Email:** henroyeffienterprise@gmail.com

**Andrew Kalu Njoku**
Department of Geology, University of Calabar, P.M.B 1115, Calabar, Cross River State, Nigeria
**Email:** askandrew4@gmail.com

**Josephine Uzibe Odey**
Department of Geology, University of Calabar, P.M.B 1115, Calabar, Cross River State, Nigeria
**Email:** odeyjosephine07@gmail.com

## 1.0 Introduction

Quartz is one of the most abundant and economically significant industrial minerals, serving as a critical raw material in high-technology industries including electronics, photovoltaic solar systems, advanced glass manufacturing, and ceramic production.
Quartz's purity, especially the amount of trace elements like Fe, Ti, Al, Ca, and Mg, is what

primarily determines its industrial feasibility. High-purity quartz (HPQ) is generally defined as quartz containing ≥99.995% $SiO_2$ with extremely low concentrations of trace impurities (Götze, 2012). Previous investigations have demonstrated that the geological environment of quartz formation strongly controls impurity incorporation, crystal defect density, and subsequent beneficiation potential.

The majority of deposits worldwide are frequently found in hydrothermal quartz veins and granitic pegmatite veins that are rich in quartz (IOTA, 2013; Norwegian Crystallites AS, 2013). These veins may also contain rutile and tourmaline. For specialised high-purity applications, only a few numbers of deposits are appropriate in terms of volume, quality, and suitability for specialised refining techniques. Refining processes must therefore be tailored to the specific impurity composition of each quartz feedstock in order to meet stringent industrial purity requirements (Haus, 2005). The economic value of HPQ is substantially higher than that of conventional quartz materials. While low-grade quartz typically sells for 15–20 USD per tonne, HPQ may reach prices exceeding 2000 USD per tonne depending on purity and application requirements.

When there are less than 50µgg-1 of structurally incorporated trace elements in quartz, it is regarded as high purity (Harben, 2002). Tourmaline/ rutile inclusions in HPQ are a key host for these high field strength trace elements (Meinheld, 2010), which may explain quartz impurities. Although some impurities can be reduced through beneficiation, intracrystalline impurities remain the primary determinant of quartz quality. Lattice-bound trace elements, submicron inclusions <1µm, and fluid and mineral micro-inclusions (>1µm) are examples of such impurities.

Furthermore, intercrystallite impurities can appear as mineral coatings or microcrystals along grain boundaries.

Fig. 1 summarizes the industrial classification of quartz quality based on impurity concentration and corresponding market value. High-purity quartz is defined as having 8–50 µgg-1 impurities (grey shaded field), as seen in Fig. 1. The finest quartz product available on the market, IOTA 8, is made from natural quartz and represents the bottom limit of 8µgg-1 (IOTA, 2013). The deposit size's projected economic limit is based on data from active quartz mine.

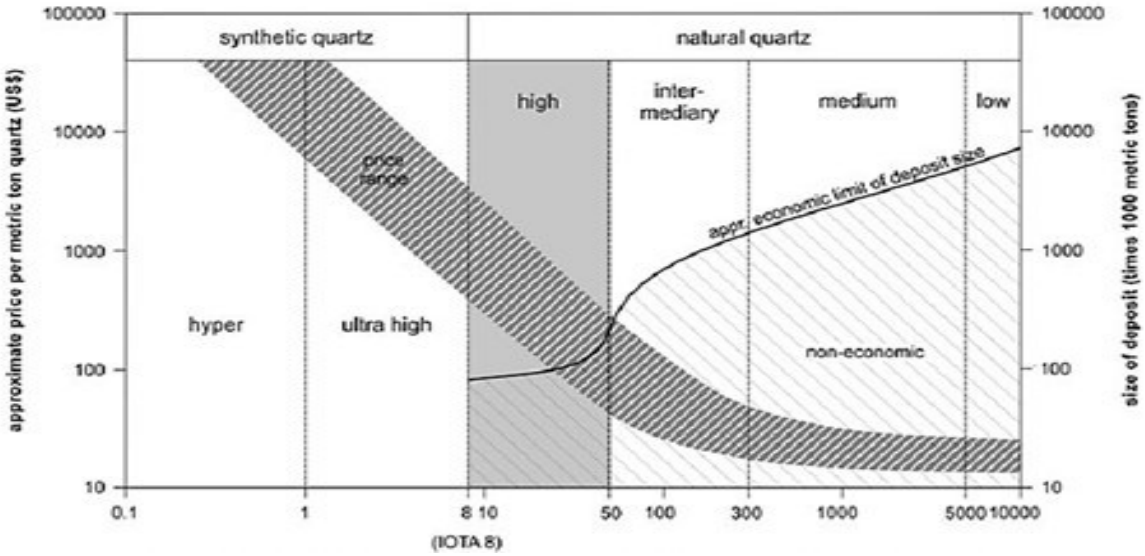


**Fig. 1: Chemical quartz quality classification (from high to low) and price range (following Harben, 2002).**

Critical elements that are detrimental to HPQ products have varying commercial concentration restrictions. The concentration limits of materials that affect the quality of melted HPQ products which are mostly silica and quartz glass products thus form the basis of the commercial description of HPQ. A preliminary effort at HPQ grading based on specific element concentration restrictions was undertaken by Müller (2012 a &

b), and Götze (2012). For Al and Ti, they recommended upper concentration limits of 25 µgg-1 and 10 µgg-1, respectively. A more thorough description of HPQ is proposed using the previously described background information, as well as the trace element concentrations of HPQ products that are currently on the market. According to Müller et al. (2012 a & b), the total of the nine elements—Na, K, Li, Al, Ca, Fe, Ti, B, and P—that are analysed on quartz crystals (single grain analysis) or processed quartz sand (bulk product analyses) should be less than 50 µgg-1.

The conceptual arrangement of these trace elements in the quartz lattice is shown in Fig. 2, and the concentrations of the IOTA standard of these nine elements and the proposed upper limits of HPQ in comparison to the average abundances in natural quartz are shown in Fig. 3. According to their average abundance in quartz (Fig. 3), the upper concentration limits suggested for Na, K, and Ca are rather high because inclusions of fluid and the most prevalent intracrystalline impurities, mica and feldspar micro-inclusions, raise the levels in processed quartz (Müller, Herrington, Armstrong, Seltmann, Kirwin, Stenina and Kronz. 2010).

With plants in North Carolina, the United States, Unimin Corp./ Sibelco continues to dominate the world's markets for high-purity quartz today. With the company's ownership shift in mid-1996, Norsk Mineral's Norwegian Crystallites, one of the few substitute suppliers, has been manufacturing high-purity quartz from its Drag plant in western Norway as well as several underground and open-pit mines (Haus and Priess, 2012). The development of possible new competitors for the global market for high-purity quartz is still ongoing. The current producing mines have an estimated shortage of roughly 15,000 tonnes, and the global market is anticipated to be over 30,000 tonnes annually for the 99.99% pure and above material (www.ngu.no). Finding additional HPQ sources is necessary, particularly in sub-Saharan African nations where solar panel use is predicted to increase exponentially in the near future. Thus, this serves as the primary driving force behind this research.

A wide variety of pegmatitic terrains can be found in Nigeria, especially in its basement complex regions, which include parts of southeast Nigeria. Large-scale granite and pegmatite intrusions have been found in the Cross River State regions of Akpet and Betem, which are located within the Oban Massif and the southeast basement complex, respectively. Although quartz-rich pegmatites are abundant in these regions, little research has been done to assess their potential as HPQ sources. It is strategically and economically important to locate and characterise indigenous sources of HPQ in Nigeria, given the need for ultra-high-purity quartz in the semiconductor and photovoltaic industries worldwide. Despite the widespread occurrence of pegmatitic quartz within Nigeria's Basement Complex, systematic mineralogical and geochemical evaluation aimed at assessing their suitability as high-purity quartz resources remains limited. In particular, comparative studies integrating genetic interpretation and impurity characterization of quartz veins within the Oban Massif are scarce.

This study aims to comparatively evaluate the geological setting, mineralogical characteristics, and trace-element geochemistry of granite-hosted pegmatite quartz veins from Akpet and Betem in southeastern Nigeria in order to assess their potential as sources of high-purity quartz for industrial applications.

Identifying indigenous HPQ resources is strategically important for Nigeria's mineral resource diversification and for supporting emerging renewable energy and semiconductor industries. Establishing the purity characteristics and beneficiation potential of local quartz deposits may reduce dependence on imported industrial silica and promote sustainable economic development.

### *1.1 Location and accessibility of the Study Area*

Fig. 4 displays a map with the study areas' locations on it. Akpet and Betem are part of the larger Nigerian Basement Complex and are located in southeast Nigeria. Scatterings of granite and related pegmatites are visible in road excavations, river cuts, and minor quarries in both locations, which are in rural upland terrain (Fig. 4). Latitudes 5°30'N to 6°00'N and longitudes 8°00'E to 8°30'E approximately match the area's coordinates. The rock types found here are pegmatites, schist, and granite. Because local communities are small, access is

usually provided by a chain of paved regional highways that connect to large urban centres, followed by rural paths and dirt district roads that go to the outcrop regions.

### *1.2 Geologic Settings*

The Congo, Kalahari, and West African cratons are the three main cratons that underlie the African continent. A network of mobile belts that were active in the late Proterozoic era divides them from one another. However, the Nigerian Basement Complex is located within a mobile belt affected by the Pan-African Orogeny (600 ± 150 Ma) to the north by the Tuareg Shield, to the south-east by the Congo Craton, and to the east by the West African Craton (Petters, 1991; Omang et al., 2024).

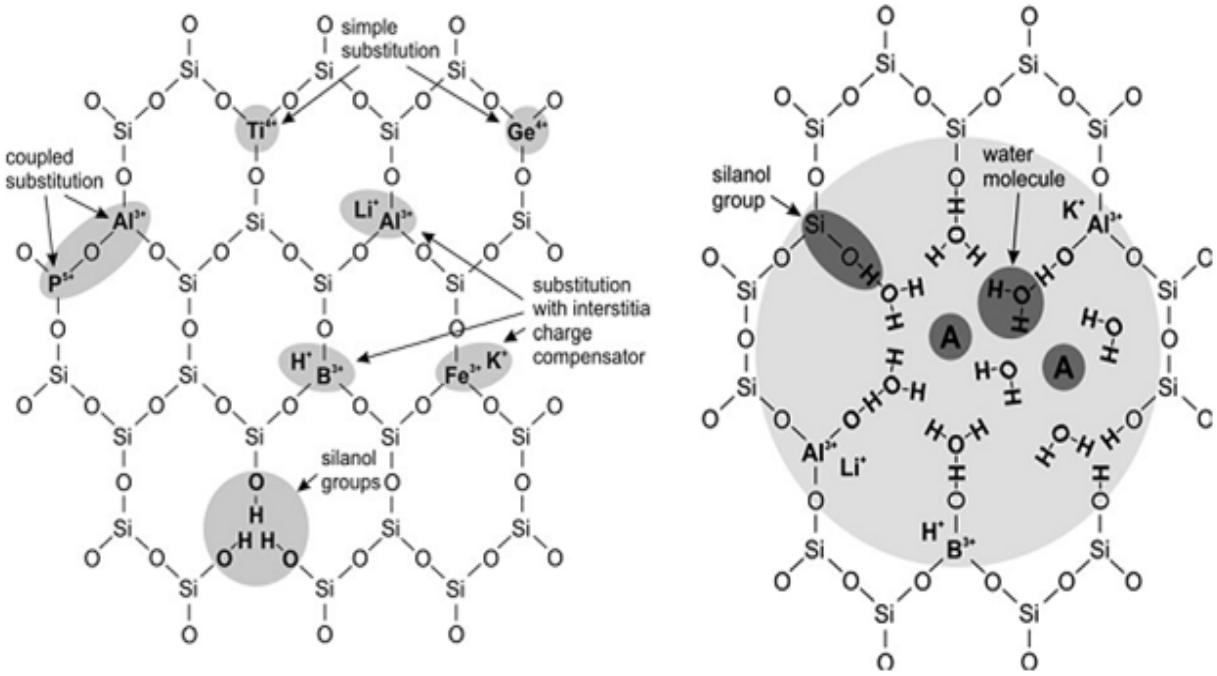


**Fig. 2 a): Diagrammatic quartz structure (adapted from Götze, 2009) illustrating the arrangement of trace elements in the quartz lattice. b) theoretical arrangement of an atomic microcluster that is mostly composed of Al, alkali ions, and H in the form of molecular water and OH. Ions like P5+, B3+, and $Fe_3^+$ that attract hydroxyls can occupy the A position. A cluster like this would signify a change from lattice errors to inclusions the size of nanometres (adapted from Müller, Armstrong, Herrington and Seltmann (2003).**

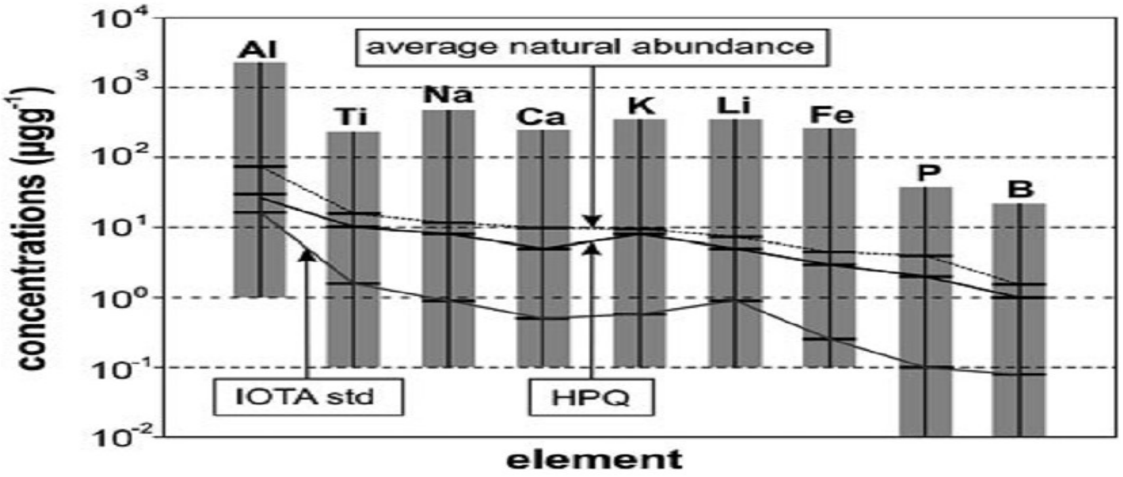


**Fig. 3: The mean quantity and fluctuations (bars) of nine detrimental trace elements in natural quartz in comparison to the recommended upper limits of HPQ and IOTA standardised quartz (IOTA 2013).**

These rocks are primarily found in the north-central and southwestern regions, with smaller amounts in the southwest and northeast, especially in the vicinity of the Obudu and Oban-massif areas (Ukaegbu & Ekwueme, 2006). Fig. 5 displays the geologic map of Nigeria, which shows the regional fractures and the locations of rare-metal and barren pegmatites (after Garba, 2003). Fig. 6 displays the geologic map of the Oban Massif.

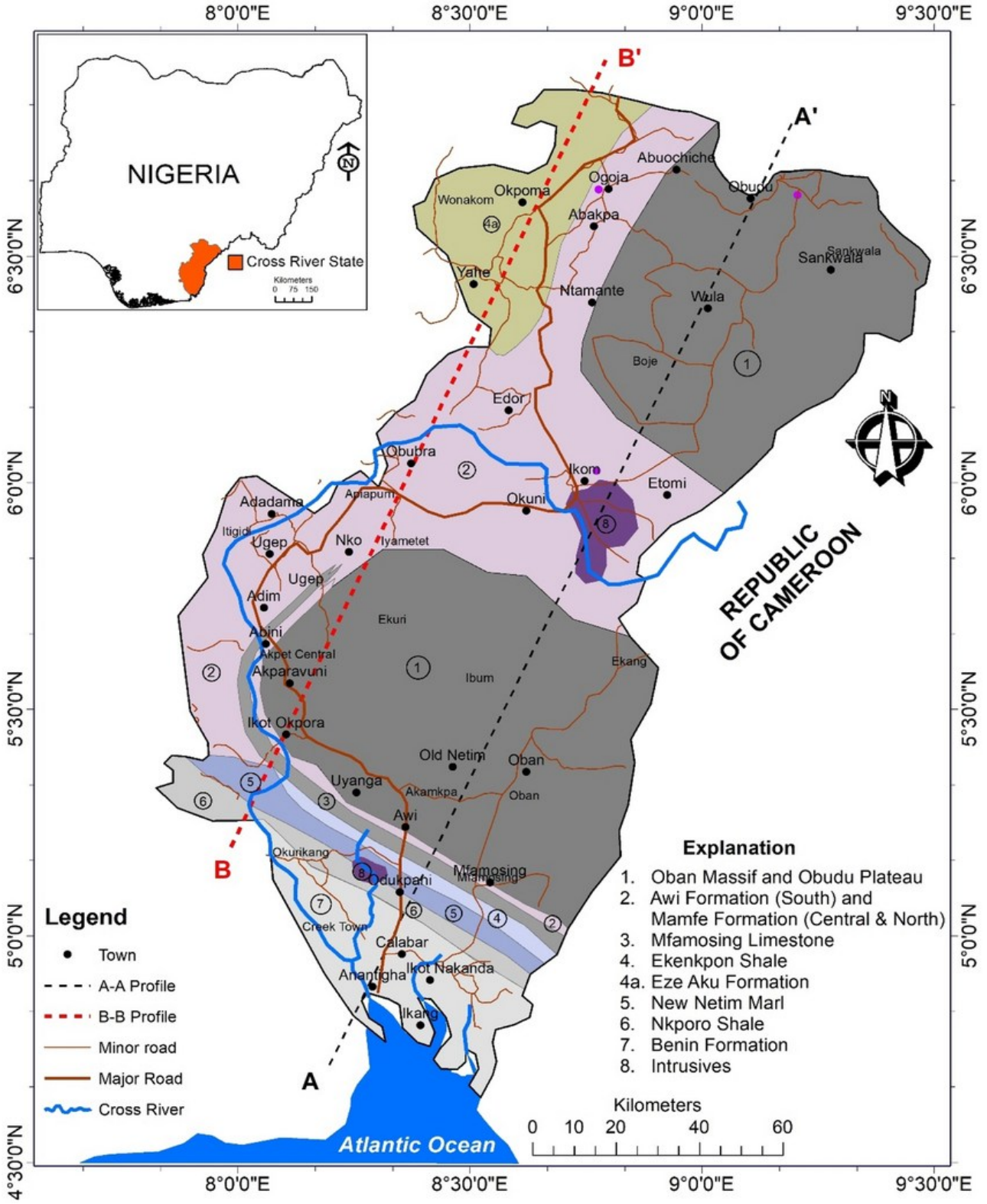


**Fig. 4: Geologic map of Cross River state, showing the study area locations (after Edet et al., 2025).**

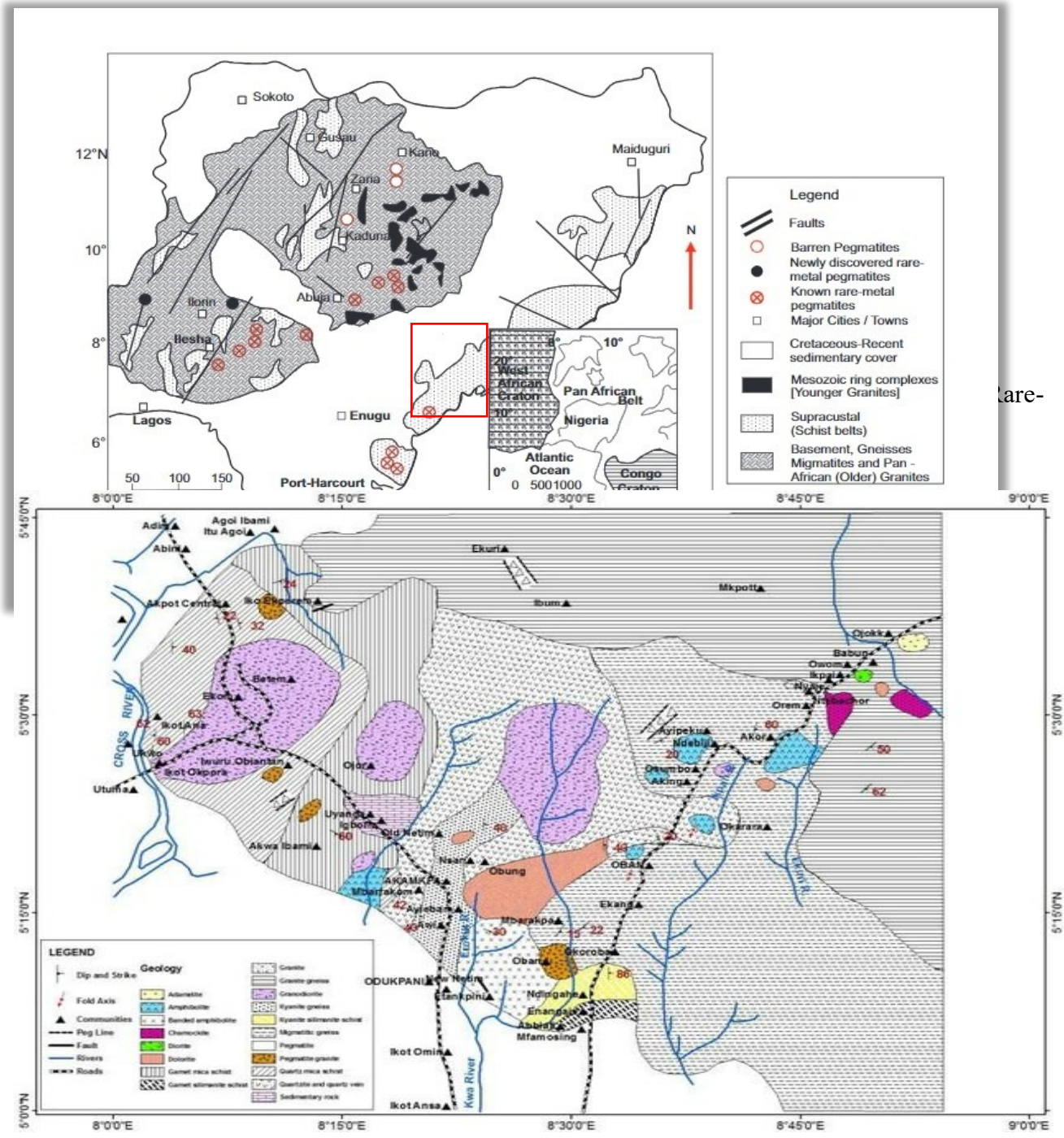


**Fig. 6: Regional Geologic map of the Oban Massif.**

The crystalline basement domain that underlies a large portion of southeast Nigeria contains the research regions. This basement is a patchwork of granitoid intrusions and metamorphic belts formed during orogenic processes, primarily the Pan-African Orogeny, which culminated in the late Proterozoic to early Paleozoic. Banded gneisses, schists, migmatites, and several generations of granitoid intrusions make up the local crust (Rahaman, 1988), residual melts, produced pegmatites with massive crystals and distinct mineral suites (Ekwueme, 1990). Regional faulting, brittle fractures, and shear zones characterised the structural plumbing, which provided pathways for hydrothermal fluids and residual melts to migrate and crystallise. Hydrothermal alteration linked to late fluids changed the wall rocks and pegmatite

margins, resulting in sericitized zones and, at times, remobilising silica and metals (Ekwueme & Matheis, 1995; Ekwueme, 1990).

From an economic standpoint, the region is favourable to a variety of pegmatite-related mineralisation, including rare-metal minerals (columbite–tantalite, cassiterite) where locally enriched, spodumene and lepidolite in lithium-rich pegmatites, and coarse quartz suitable for industrial-grade material. According to Egesi and Ukaegbu (2010), the possibility of high-purity quartz depends on two factors: primary magmatic processes that produce large, inclusion-poor crystals and subsequent weathering or alteration that can either increase or decrease the purity of quartz by introducing impurities such as iron.

Biotite-muscovite granites, migmatitic gneisses, and vast networks of pegmatite and quartz veins form the foundation of the Akpet region. The pegmatites in this area are typically coarse-grained and mostly consist of quartz, feldspar (albite and microcline), and muscovite, with garnet and tourmaline serving as accessory minerals. These pegmatites cut discordantly across the host granite as dykes, irregular veins, and pods. The pegmatites' structural orientations, which are governed by pre-existing Pan-African deformational fabrics, are NE-SW and NW-SE.

Late-stage infusion of volatile-rich pegmatitic melts was made easier by these structural weaknesses (Rahaman, 1988).

Though it has more varied pegmatitic textures and compositions, Betem, which is located west of Akpet along the same Oban Massif corridor, has a comparable geological structure. Numerous quartz-rich pegmatite veins break through the biotite-rich granites and tonalitic to granodioritic gneisses that make up the host rocks. Hydrothermal overprinting is frequently visible in Betem quartz crystals, as evidenced by secondary mineral development and recrystallisation textures, which may have a local impact on purity. Beryl, tourmaline (schorl), kaolinite (alteration product), and trace amounts of columbite-tantalite are examples of accessory minerals.

## 2.0 Materials and Method

This study employed a multidisciplinary approach—including field mapping, petrographic examination, geochemical analysis, and advanced mineralogical characterization—to evaluate the mineralogical composition, trace-element distribution, and potential industrial quality of quartz in the Akpet and Betem pegmatites.

The overall workflow of sample collection, preparation, and analytical procedures used in this study is illustrated in Fig. 7. Thirty representative quartz samples—15 from each site, Akpet and Betem—were collected and subsequently prepared in the Geology Laboratory of the University of Calabar for mineralogical and geochemical analysis. The samples were air-dried at room temperature for two weeks to ensure removal of moisture prior to mechanical crushing. Dried samples were initially crushed using a jaw crusher fitted with a 10-mesh screen to produce particles smaller than 2 mm.

The crushed material was quartered and further pulverized in a porcelain mortar to achieve a particle size of 200 mesh (<75 μm), ensuring homogenization suitable for geochemical and mineralogical analyses. The pulverized samples were thoroughly homogenized to minimize sample heterogeneity and ensure consistent analytical results.

Once the desired particle size was achieved, the material was thoroughly re-homogenized to eliminate any potential discrepancies.

Approximately 30 g of each homogenized sample were weighed, labeled, and sealed in pharmaceutical-grade bags to preserve their chemical integrity until geochemical analysis.

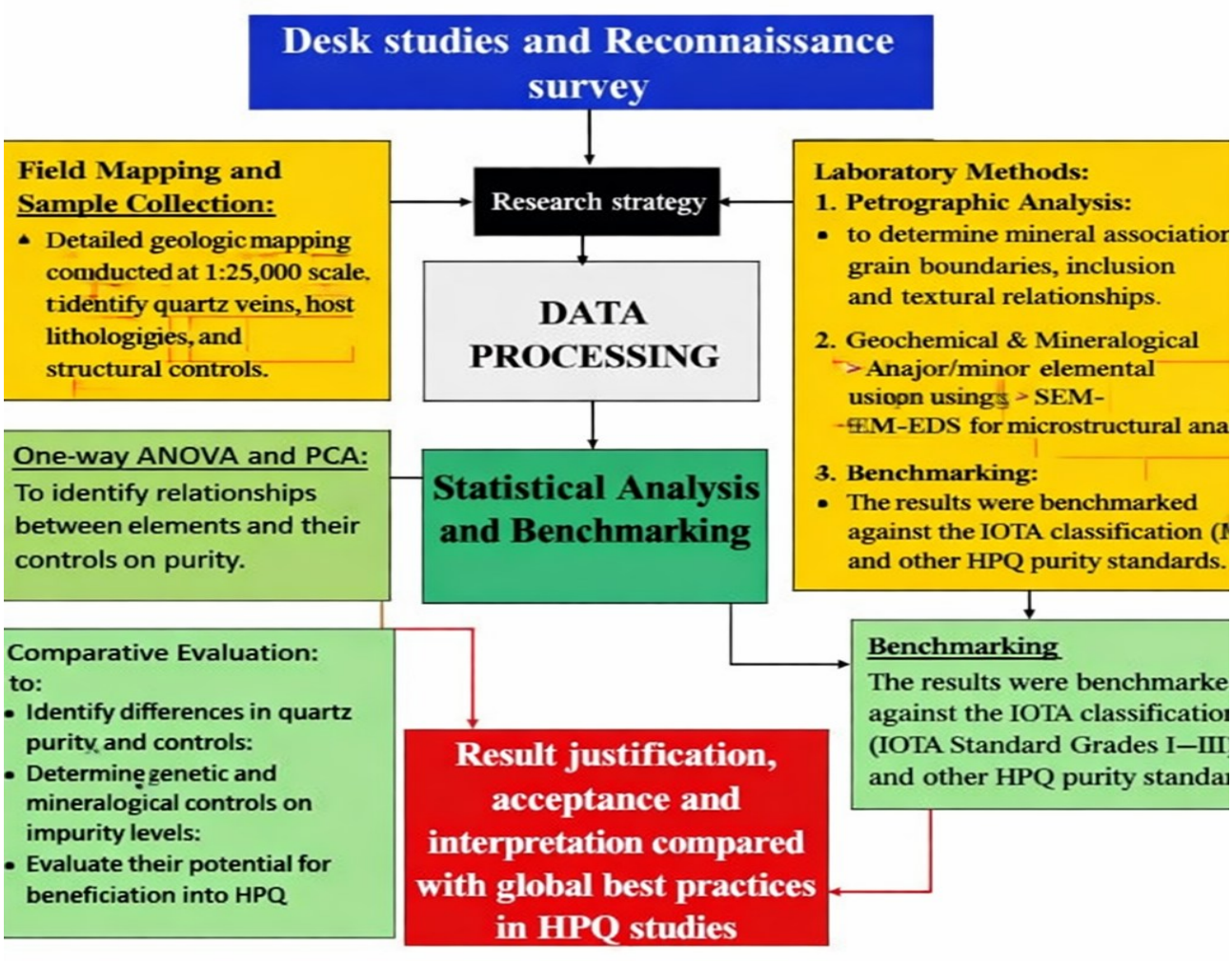


**Fig. 7: Workflow of the methods used in the present study**

All sample preparation procedures were conducted in accordance with standardized laboratory protocols to ensure the reliability and reproducibility of analytical results.

## 3.0 Results and Discussion

### *3.1 ICP-MS results of the bulk chemistry of Akpet and Betem quartz samples*

Tables 1 and 2 show the ICP-MS results of quartz samples from the Akpet and Betem areas, respectively. Key major oxide and trace element trends are illustrated in Figs 8–12 for comparative analysis." This corrects grammar and adds clarity. Figs 8 - 9, and 10 – 11 shows graphical variation…" with "Figs 8–11 show the variation of major oxides and trace elements in Akpet and Betem quartz samples, while Fig. 12 compares trace element distributions between the two areas.

### *3.2 Petrography*

#### *3.2.1 Petrography of pegmatite-hosted quartz from Akpet*

The photomicrographs in Figs 13 and 14 (a–d), showing both PPL and CPL views, illustrate quartz bodies from the Akpet area. The observed mineralogical and textural features provide valuable insights into the petrogenesis and composition of the pegmatite-hosted quartz veins and associated feldspars. For example, photomicrograph Plate 1a (MG: ×40, PPL) reveals textural patterns indicative of hydrothermal or metamorphic formation. The presence of magnetite inclusions within the quartz suggests crystallization from iron-rich fluids and points to an environment that experienced transitions between reducing and oxidizing conditions during quartz formation.

#### *3.2.2 Quartz Purity and Elemental Composition*

Quartz samples from the Akpet area contain minor impurities, including Al, Fe, Ca, Mg, and K.

**Table 1: ICP-MS results of the bulk chemistry of quartz samples from the Akpet area**

| | Akp1 | Akp2 | Akp3 | Akp4 | Akp5 | Akp6 | Akp7 | Akp8 | Akp9 | Akp10 | Akp11 | Akp12 | Akp13 | Akp14 | Akp15 | Min | Max | Mean |
|---|---|---|---|---|---|---|---|---|---|---|---|---|---|---|---|---|---|---|
| **Major Oxides (wt%)** | | | | | | | | | | | | | | | | | | |
| $SiO_2$ | 98.01 | 97.44 | 97.01 | 97.44 | 97.22 | 96.77 | 98 | 97.01 | 94.23 | 98.01 | 97.33 | 98.01 | 98.01 | 97.23 | 98.01 | 94.23 | 98.01 | 97.31 |
| $Al_2O_3$ | 0.56 | 0.5 | 0.56 | 0.55 | 0.51 | 0.55 | 0.5 | 0.56 | 0.52 | 0.5 | 0.5 | 0.52 | 0.5 | 0.56 | 0.59 | 0.5 | 0.59 | 0.53 |
| $Fe_2O_3$(T) | 0.1 | 0.5 | 0.45 | 0.41 | 0.12 | 0.34 | 0.03 | 0.12 | 0.31 | 0.02 | 0.1 | 0.02 | 0.03 | 0.29 | 0.11 | 0.02 | 0.5 | 0.19 |
| MnO | 0.01 | 0.01 | 0.001 | 0.01 | 0.02 | 0.007 | 0.002 | 0.012 | 0.004 | 0.005 | 0.001 | 0.02 | 0.003 | 0.02 | 0.01 | 0.001 | 0.02 | 0.009 |
| MgO | 0.03 | 0.03 | 0.03 | 0.04 | 0.04 | 0.04 | 0.1 | 0.19 | 0.28 | 0.21 | 0.21 | 0.07 | 0.33 | 0.04 | 0.04 | 0.03 | 0.33 | 0.12 |
| CaO | 0.01 | 0.01 | 0.02 | 0.02 | 0.02 | 0.03 | 0.003 | 0.06 | 0.04 | 0.1 | 0.13 | 0.02 | 0.03 | 0.13 | 0.1 | 0.003 | 0.13 | 0.048 |
| $Na_2O$ | 0.08 | 0.42 | 0.65 | 0.45 | 0.51 | 0.55 | 0.52 | 0.55 | 0.52 | 0.5 | 0.54 | 0.51 | 0.51 | 0.51 | 0.51 | 0.08 | 0.65 | 0.48 |
| $K_2O$ | 0.5 | 0.54 | 0.51 | 0.55 | 0.53 | 0.56 | 0.54 | 0.56 | 0.51 | 0.56 | 0.58 | 0.55 | 0.56 | 0.61 | 0.57 | 0.5 | 0.61 | 0.54 |
| $TiO_2$ | 0.01 | 0.01 | 0.01 | 0.01 | 0.01 | 0.01 | 0.002 | 0.003 | 0.01 | 0.004 | 0.012 | 0.03 | 0.01 | 0.31 | 0.003 | 0.002 | 0.31 | 0.029 |
| $P_2O_5$ | 0.01 | 0.01 | 0.01 | 0.07 | 0.09 | 0.1 | 0.04 | 0.1 | 0.1 | 0.01 | 0.1 | 0.02 | 0.01 | 0.2 | 0.01 | 0.01 | 0.2 | 0.058 |
| LOI | 0.01 | 0.18 | 0.36 | 0.53 | 0.43 | 0.88 | 1.15 | 1.79 | 2.43 | 3.07 | 3.71 | 4.36 | 4.41 | 3.6 | 2.78 | 0.01 | 4.41 | 1.979 |
| Total | 99.32 | 99.47 | 99.251 | 99.55 | 99.07 | 98.957 | 99.737 | 99.165 | 96.524 | 99.919 | 99.503 | 99.77 | 99.993 | 99.9 | 99.953 | 96.524 | 99.993 | 99.33 |

| | Akp1 | Akp2 | Akp3 | Akp4 | Akp5 | Akp6 | Akp7 | Akp8 | Akp9 | Akp10 | Akp11 | Akp12 | Akp13 | Akp14 | Akp15 | Min | Max | Mean |
|---|---|---|---|---|---|---|---|---|---|---|---|---|---|---|---|---|---|---|
| Trace elements ($\mu g\text{-}g^{-1}$) | | | | | | | | | | | | | | | | | | |
| Au | 3 | 2.56 | 2.11 | 1.67 | 1.22 | 0.78 | 0.42 | 0.43 | 0.43 | 0.44 | 0.44 | 0.45 | 0.71 | 1.36 | 2 | 0.42 | 3 | 1.201333 |
| Ag | 0.2 | 0.24 | 0.27 | 0.31 | 0.34 | 0.38 | 0.41 | 0.4 | 0.4 | 0.39 | 0.39 | 0.38 | 0.38 | 0.38 | 0.39 | 0.2 | 0.41 | 0.350667 |
| As | 1.5 | 1.52 | 1.53 | 1.55 | 1.57 | 1.59 | 1.6 | 1.62 | 1.64 | 1.66 | 1.67 | 1.69 | 1.62 | 1.41 | 1.2 | 1.2 | 1.69 | 1.558 |
| Ba | 4 | 15.21 | 26.41 | 37.62 | 48.83 | 60.03 | 71.83 | 85.97 | 100.1 | 114.24 | 128.38 | 142.52 | 140.72 | 115.01 | 89.3 | 4 | 142.52 | 78.678 |
| Be | 0.8 | 19.97 | 39.14 | 58.32 | 77.49 | 96.66 | 108.69 | 92.14 | 75.59 | 59.03 | 42.48 | 25.93 | 14.95 | 12.33 | 9.71 | 0.8 | 108.69 | 48.882 |
| Bi | 1.6 | 1.58 | 1.57 | 1.55 | 1.53 | 1.51 | 1.5 | 1.52 | 1.54 | 1.56 | 1.57 | 1.59 | 3.97 | 9.9 | 15.83 | 1.5 | 15.83 | 3.221333 |
| Br | 2 | 1.81 | 1.62 | 1.43 | 1.24 | 1.05 | 0.89 | 0.86 | 0.82 | 0.79 | 0.76 | 0.72 | 0.71 | 0.72 | 0.74 | 0.71 | 2 | 1.077333 |
| Cd | 0.8 | 0.73 | 0.66 | 0.59 | 0.52 | 0.46 | 0.4 | 0.38 | 0.36 | 0.34 | 0.33 | 0.31 | 0.38 | 0.59 | 0.8 | 0.31 | 0.8 | 0.51 |
| Co | 0.3 | 0.59 | 0.89 | 1.18 | 1.47 | 1.77 | 2.24 | 3.45 | 4.66 | 5.86 | 7.07 | 8.28 | 8.52 | 7.31 | 6.1 | 0.3 | 8.52 | 3.979333 |
| Cr | 381 | 334.62 | 288.24 | 241.86 | 195.48 | 149.1 | 117.83 | 146.97 | 176.1 | 205.24 | 234.38 | 263.52 | 288.72 | 308.03 | 327.34 | 117.83 | 381 | 243.8953 |
| Cs | 0.4 | 8.09 | 15.78 | 23.47 | 31.16 | 38.85 | 44.36 | 41.17 | 37.98 | 34.79 | 31.6 | 28.41 | 23.23 | 19.23 | 102.23 | 0.4 | 102.23 | 32.05 |
| Cu | 9 | 8.66 | 8.31 | 7.97 | 7.62 | 7.28 | 7.45 | 9.69 | 11.93 | 14.17 | 16.41 | 18.66 | 19.38 | 17.83 | 16.28 | 7.28 | 19.38 | 12.04267 |

ZZ

| | | | | | | | | | | | | | | | | | | |
|---|---|---|---|---|---|---|---|---|---|---|---|---|---|---|---|---|---|---|
| Hf | 0.3 | 0.234 | 1.23 | 1.003 | 0.723 | 1.23 | 2.23 | 1.23 | 1.44 | 1.23 | 2.33 | 0.23 | 0.43 | 0.83 | 1.23 | 0.23 | 2.33 | 1.06 |
| Ni | 12 | 11.14 | 10.28 | 9.41 | 8.55 | 7.69 | 7.79 | 11.76 | 15.72 | 19.69 | 23.66 | 27.62 | 28.69 | 25.41 | 22.14 | 7.69 | 28.69 | 16.10333 |
| Pb | 4 | 7.1 | 10.21 | 13.31 | 16.41 | 19.52 | 21.66 | 19.93 | 18.21 | 16.48 | 14.76 | 13.03 | 12.34 | 15.23 | 14.23 | 4 | 21.66 | 14.42 |
| Rb | 15 | 177.93 | 340.86 | 503.79 | 666.72 | 829.66 | 933.79 | 802.76 | 671.72 | 540.69 | 409.66 | 278.62 | 321 | 102.2 | 91.2 | 15 | 933.79 | 445.70 |
| S | 1.2 | 1.03 | 0.987 | 0.89 | 1.34 | 2.21 | 1.32 | 1.87 | 0.87 | 1.22 | 1.54 | 2.22 | 1.87 | 3.44 | 2.12 | 0.87 | 3.44 | 1.608 |
| Sb | 0.3 | 0.4 | 0.51 | 0.61 | 0.71 | 0.82 | 0.9 | 0.9 | 0.9 | 0.9 | 0.9 | 0.9 | 0.85 | 0.73 | 0.61 | 0.3 | 0.9 | 0.729 |
| Se | 2.5 | 2.6 | 2.7 | 2.8 | 2.3 | 2.5 | 2.8 | 2.2 | 2.3 | 3.4 | 2.1 | 2.3 | 3.3 | 2.4 | 2.6 | 2.1 | 3.4 | 2.586 |
| Sr | 5 | 8.97 | 12.93 | 16.9 | 20.86 | 24.83 | 27.72 | 26.34 | 24.97 | 23.59 | 22.21 | 20.83 | 19.66 | 21.54 | 20.86 | 5 | 27.72 | 19.814 |
| Ta | 0.8 | 2.04 | 3.28 | 4.52 | 5.77 | 7.01 | 7.83 | 6.97 | 6.1 | 5.24 | 4.38 | 3.52 | 4.5 | 6.6 | 5.3 | 0.8 | 7.83 | 4.924 |
| Th | 0.4 | 0.3 | 0.4 | 0.2 | 0.3 | 0.4 | 0.5 | 0.4 | 0.3 | 0.2 | 0.4 | 0.5 | 0.5 | 0.7 | 0.9 | 0.2 | 0.9 | 0.426 |
| U | 0.3 | 0.51 | 0.71 | 0.92 | 1.13 | 1.33 | 1.58 | 1.98 | 2.37 | 2.77 | 3.17 | 3.56 | 3.95 | 4.33 | 4.71 | 0.3 | 4.71 | 2.221 |
| V | 6 | 7.2 | 5 | 6 | 7.2 | 5.5 | 6.3 | 7.3 | 6.5 | 5.5 | 4.8 | 6.2 | 5.8 | 4.9 | 6.2 | 4.8 | 7.3 | 6.02 |
| Zn | 10 | 13.62 | 17.24 | 20.86 | 24.48 | 28.1 | 31.9 | 36.38 | 40.86 | 45.34 | 49.83 | 54.31 | 53.34 | 44.21 | 35.07 | 10 | 54.31 | 33.702 |
| Zr | 4 | 4.52 | 5.03 | 5.55 | 6.07 | 6.59 | 11.1 | 31.62 | 52.14 | 72.66 | 93.17 | 113.69 | 117.59 | 96.55 | 75.52 | 4 | 117.59 | 46.38 |
| La | 0.9 | 0.99 | 1.07 | 1.16 | 1.24 | 1.33 | 2.23 | 1.23 | 2.1 | 3.23 | 2.12 | 3.23 | 1.23 | 3.23 | 1.23 | 0.9 | 3.23 | 1.768 |
| Ce | 10.23 | 9.23 | 7.23 | 6.12 | 8.22 | 34.23 | 5.17 | 16.03 | 26.9 | 37.76 | 48.62 | 59.48 | 41.23 | 28.23 | 31.23 | 5.17 | 59.48 | 24.66 |
| Al | 10.3 | 8.7 | 10.2 | 9.2 | 11.3 | 10.3 | 10.1 | 9.3 | 8.7 | 9.3 | 10.2 | 11.3 | 9.3 | 8.3 | 10.3 | 8.3 | 11.3 | 9.786 |
| Ti | 1.7 | 1.4 | 2.1 | 2.3 | 2.4 | 1.5 | 1.4 | 2.1 | 1.4 | 3.4 | 3.3 | 1.2 | 1.5 | 1.4 | 1.5 | 1.2 | 3.4 | 1.906 |
| Na | 0.2 | 0.56 | 0.87 | 0.3 | 0.5 | 0.4 | 0.3 | 0.2 | 0.56 | 1.2 | 0.4 | 0.8 | 0.4 | 0.3 | 0.4 | 0.2 | 1.2 | 0.492 |
| Ca | 3.4 | 3.8 | 3.8 | 3.9 | 4.2 | 6.3 | 2.6 | 3.4 | 3.8 | 2.5 | 2.7 | 5.3 | 8.3 | 3.3 | 6.3 | 2.5 | 8.3 | 4.24 |
| K | 1.4 | 1.3 | 1.3 | 1.4 | 1.7 | 2.1 | 1.5 | 1.8 | 1.3 | 1.3 | 2.1 | 2.2 | 2.1 | 1.5 | 2.1 | 1.3 | 2.2 | 1.67 |
| Li | 0.32 | 1.32 | 1.76 | 1.44 | 1.65 | 1.55 | 2 | 1.33 | 0.98 | 0.56 | 0.32 | 0.43 | 0.43 | 1.65 | 1.88 | 0.32 | 2 | 1.17 |
| Fe | 2.6 | 3.4 | 3.1 | 2.7 | 3.2 | 3.11 | 3.4 | 2.1 | 3.4 | 4.2 | 2.5 | 3.1 | 4.21 | 3.4 | 2.11 | 2.1 | 4.21 | 3.102 |
| B | 1.5 | 3.2 | 2.1 | 3.2 | 2.9 | 2.7 | 1.77 | 2.11 | 1.89 | 3.22 | 2.45 | 2.23 | 3.21 | 1.88 | 2.98 | 1.5 | 3.22 | 2.48 |
| Ge | 0.1 | 0.21 | 0.32 | 0.12 | 1.43 | 0.87 | 0.21 | 0.21 | 0.33 | 0.12 | 0.32 | 0.12 | 0.54 | 0.65 | 0.12 | 0.1 | 1.43 | 0.378 |

| | Akp1 | Akp2 | Akp3 | Akp4 | Akp5 | Akp6 | Akp7 | Akp8 | Akp9 | Akp10 | Akp11 | Akp12 | Akp13 | Akp14 | Akp15 | Min | Max | Mean |
|---|---|---|---|---|---|---|---|---|---|---|---|---|---|---|---|---|---|---|
| Light Rare Earth Elements (µg-g$^{-1}$) | | | | | | | | | | | | | | | | | | |
| Sc | 0.2 | 0.3 | 0.41 | 0.51 | 0.61 | 0.72 | 1.09 | 2.56 | 4.02 | 5.49 | 6.96 | 8.42 | 8.67 | 7.1 | 5.53 | 0.2 | 8.67 | 3.506 |
| Sm | 0.2 | 0.22 | 0.23 | 0.25 | 0.27 | 0.29 | 0.52 | 1.6 | 2.69 | 3.78 | 4.86 | 5.95 | 6.16 | 5.06 | 3.95 | 0.2 | 6.16 | 2.402 |

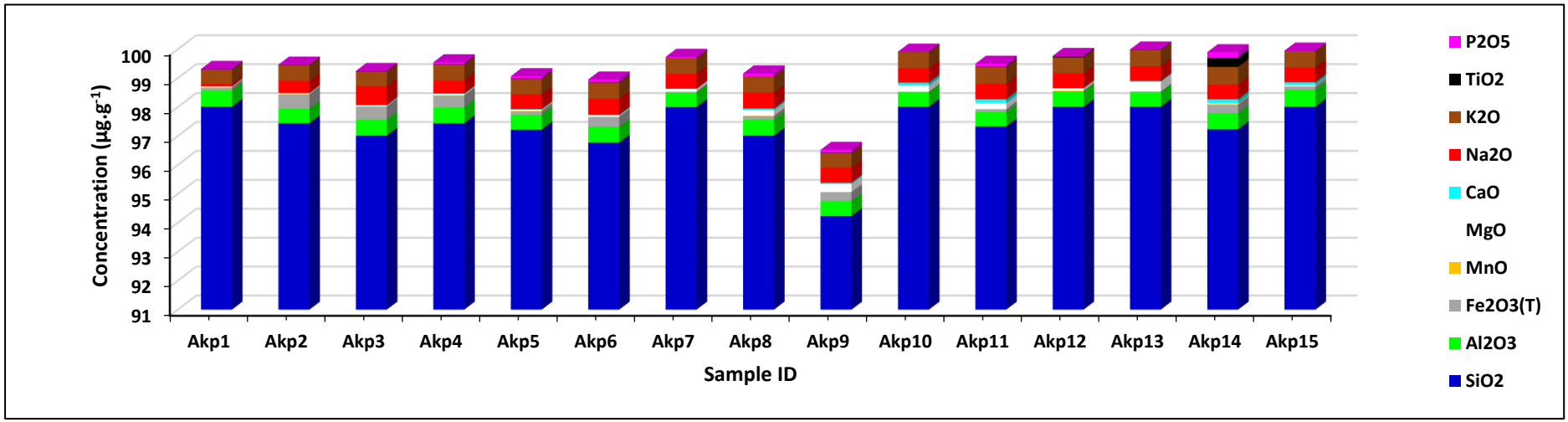


**Fig. 8: Graphical variation in major oxides from the Akpet area**

**Fig. 9: Graphical variation in trace elements from the Akpet area**

**Table 2: ICP-MS results of the bulk chemistry of quartz samples from the Betem area**

| | Bet1 | Bet2 | Bet3 | Bet4 | Bet5 | Bet6 | Bet7 | Bet8 | Bet9 | Bet10 | Bet11 | Bet12 | Bet13 | Bet14 | Bet15 | Min | Max | Mean |
|---|---|---|---|---|---|---|---|---|---|---|---|---|---|---|---|---|---|---|
| Major (wt%) | Oxides | | | | | | | | | | | | | | | | | |
| $SiO_2$ | 95.01 | 95.08 | 95.02 | 95.06 | 95.004 | 95.02 | 95.22 | 95.11 | 95.12 | 95.02 | 95.03 | 95.08 | 95.02 | 95.02 | 95.01 | 95.004 | 95.22 | 95.05493 |
| $Al_2O_3$ | 2.03 | 2.01 | 2.03 | 2.006 | 2.01 | 2.01 | 2.03 | 2.009 | 2.11 | 2.02 | 2.003 | 2.01 | 2.03 | 2.01 | 2.03 | 2.003 | 2.11 | 2.0232 |
| $Fe_2O_3$(T) | 0.21 | 0.2 | 0.21 | 0.2 | 0.21 | 0.32 | 0.21 | 0.21 | 0.201 | 0.22 | 0.2 | 0.2 | 0.21 | 0.32 | 0.21 | 0.2 | 0.32 | 0.222067 |
| MnO | 0.01 | 0.02 | 0.01 | 0.01 | 0.01 | 0.01 | 0.01 | 0.012 | 0.01 | 0.03 | 0.01 | 0.02 | 0.01 | 0.01 | 0.01 | 0.01 | 0.03 | 0.0128 |
| MgO | 0.2 | 0.19 | 0.2 | 0.2 | 0.22 | 0.21 | 0.22 | 0.2 | 0.23 | 0.24 | 0.2 | 0.19 | 0.2 | 0.21 | 0.2 | 0.19 | 0.24 | 0.207333 |
| CaO | 0.1 | 0.1 | 0.1 | 0.1 | 0.12 | 0.12 | 0.11 | 0.13 | 0.12 | 0.14 | 0.1 | 0.1 | 0.1 | 0.12 | 0.1 | 0.1 | 0.14 | 0.110667 |
| $Na_2O$ | 1.04 | 1.03 | 1.03 | 1.05 | 1.002 | 1.004 | 1.03 | 1.002 | 1.01 | 1.02 | 1.002 | 1.03 | 1.03 | 1.004 | 1.04 | 1.002 | 1.05 | 1.0216 |
| $K_2O$ | 1.02 | 1.02 | 1.03 | 1.001 | 1.003 | 1.02 | 1.03 | 1.003 | 1.002 | 1.003 | 1.02 | 1.02 | 1.03 | 1.02 | 1.02 | 1.001 | 1.03 | 1.016133 |
| $TiO_2$ | 0.01 | 0.01 | 0.01 | 0.001 | 0.002 | 0.03 | 0.03 | 0.001 | 0.03 | 0.04 | 0.01 | 0.01 | 0.01 | 0.03 | 0.01 | 0.001 | 0.04 | 0.0156 |
| $P_2O_5$ | 0.1 | 0.1 | 0.1 | 0.1 | 0.01 | 0.01 | 0.01 | 0.01 | 0.01 | 0.01 | 0.002 | 0.1 | 0.1 | 0.01 | 0.1 | 0.002 | 0.1 | 0.051467 |

| | | | | | | | | | | | | | | | | | | |
|---|---|---|---|---|---|---|---|---|---|---|---|---|---|---|---|---|---|---|
| LOI | 1.97 | 1.15 | 0.34 | 0.01 | 0.01 | 0.01 | 0.01 | 0.01 | 0.01 | 0.89 | 1.98 | 3.08 | 4.18 | 5.27 | 6.37 | 0.01 | 6.37 | 1.686 |
| Total | 99.73 | 99.76 | 99.74 | 99.728 | 99.591 | 99.754 | 99.9 | 99.687 | 99.843 | 99.743 | 99.577 | 99.76 | 99.74 | 99.754 | 99.73 | 99.577 | 99.9 | 99.7358 |

| | Bet1 | Bet2 | Bet3 | Bet4 | Bet5 | Bet6 | Bet7 | Bet8 | Bet9 | Bet10 | Bet11 | Bet12 | Bet13 | Bet14 | Bet15 | Min | Max | Mean |
|---|---|---|---|---|---|---|---|---|---|---|---|---|---|---|---|---|---|---|
| Trace elements ($\mu g\text{-}g^{-1}$) | | | | | | | | | | | | | | | | | | |
| Au | 2.65 | 3.29 | 3.94 | 4.18 | 4.14 | 4.11 | 4.08 | 4.04 | 4.01 | 4 | 4 | 4 | 4 | 4 | 4 | 2.65 | 4.18 | 3.896 |
| Ag | 0.39 | 0.4 | 0.4 | 0.39 | 0.37 | 0.36 | 0.34 | 0.32 | 0.3 | 0.31 | 0.33 | 0.35 | 0.37 | 0.38 | 0.4 | 0.3 | 0.4 | 0.360667 |
| As | 1 | 0.79 | 0.58 | 0.63 | 0.86 | 1.08 | 1.31 | 1.53 | 1.76 | 1.62 | 1.4 | 1.17 | 0.95 | 0.72 | 0.5 | 0.5 | 1.76 | 1.06 |
| Ba | 63.6 | 37.89 | 12.18 | 2.01 | 2.2 | 2.39 | 2.58 | 2.77 | 2.96 | 2.79 | 2.53 | 2.28 | 2.02 | 1.76 | 1.5 | 1.5 | 63.6 | 9.430667 |
| Be | 7.09 | 4.47 | 1.85 | 0.79 | 0.77 | 0.76 | 0.74 | 0.72 | 0.7 | 43.22 | 96.38 | 149.53 | 202.69 | 255.84 | 309 | 0.7 | 309 | 71.63667 |
| Bi | 21.77 | 27.7 | 33.63 | 32.44 | 26.51 | 20.58 | 14.65 | 8.72 | 2.79 | 3.86 | 6.69 | 9.52 | 12.34 | 15.17 | 18 | 2.79 | 33.63 | 16.958 |
| Br | 0.76 | 0.78 | 0.79 | 0.8 | 0.8 | 0.8 | 0.8 | 0.8 | 0.8 | 0.91 | 1.05 | 1.19 | 1.32 | 1.46 | 1.6 | 0.76 | 1.6 | 0.977333 |
| Cd | 1 | 1.21 | 1.42 | 1.38 | 1.17 | 0.96 | 0.76 | 0.55 | 0.34 | 0.38 | 0.49 | 0.59 | 0.69 | 0.8 | 0.9 | 0.34 | 1.42 | 0.842667 |
| Co | 4.9 | 3.69 | 2.48 | 1.9 | 1.72 | 1.55 | 1.38 | 1.21 | 1.03 | 4.31 | 8.45 | 12.59 | 16.72 | 20.86 | 25 | 1.03 | 25 | 7.186 |
| Cr | 346.66 | 365.97 | 385.28 | 369.21 | 329.55 | 289.9 | 250.24 | 210.59 | 170.93 | 178.72 | 198.38 | 218.03 | 237.69 | 257.34 | 277 | 170.93 | 385.28 | 272.366 |
| Cs | 14.22 | 15.23 | 18.34 | 19.23 | 12.22 | 11.23 | 13.44 | 10.23 | 11.23 | 3.81 | 7.83 | 11.85 | 15.87 | 19.88 | 23.9 | 3.81 | 23.9 | 13.90067 |
| Trace elements (cont'd.) | | | | | | | | | | | | | | | | | | |
| Cu | 14.72 | 13.17 | 11.62 | 10.38 | 9.34 | 8.31 | 7.28 | 6.24 | 5.21 | 9.83 | 15.86 | 21.9 | 27.93 | 33.97 | 40 | 5.21 | 40 | 15.71733 |
| Hf | 2.21 | 3.22 | 3.23 | 3.12 | 2.12 | 2.34 | 2.88 | 2.91 | 1.22 | 3.12 | 3.28 | 3.43 | 3.59 | 3.74 | 3.9 | 1.22 | 3.9 | 2.954 |
| Ni | 18.86 | 15.59 | 12.31 | 9.86 | 7.97 | 6.07 | 4.17 | 2.28 | 0.38 | 4.83 | 10.86 | 16.9 | 22.93 | 28.97 | 35 | 0.38 | 35 | 13.132 |
| Pb | 16.22 | 11.23 | 16.23 | 11.23 | 13.23 | 12.44 | 14.45 | 17.23 | 18.23 | 21.12 | 23.23 | 31.23 | 21.23 | 19.23 | 16 | 11.23 | 31.23 | 17.502 |
| Rb | 102 | 105 | 109 | 91.2 | 78.3 | 123 | 112 | 103 | 92.3 | 102 | 112 | 102 | 112 | 130 | 170 | 78.3 | 170 | 109.5867 |
| S | 4.87 | 5.54 | 4.99 | 6.54 | 5.88 | 6.17 | 5.77 | 4.23 | 5.65 | 5.54 | 4.98 | 7.87 | 6.22 | 5.12 | 6.11 | 4.23 | 7.87 | 5.698667 |
| Sb | 0.49 | 0.37 | 0.25 | 0.3 | 0.43 | 0.54 | 0.21 | 0.11 | 0.23 | 0.56 | 0.23 | 0.11 | 0.12 | 0.34 | 0.4 | 0.11 | 0.56 | 0.312667 |
| Se | 3.4 | 2.4 | 2.1 | 2.5 | 2.2 | 2.5 | 3.2 | 2.8 | 2.7 | 2.1 | 3.2 | 2.1 | 2.3 | 2.9 | 2.3 | 2.1 | 3.4 | 2.58 |
| Sr | 21.65 | 20.76 | 22.54 | 22.54 | 23.76 | 21.6 | 23.54 | 19.09 | 21.32 | 20.54 | 19.65 | 21.55 | 20.76 | 21.23 | 27 | 19.09 | 27 | 21.83533 |
| Ta | 6.2 | 5.3 | 6.2 | 5.4 | 5.6 | 3.4 | 4.4 | 5.4 | 6.4 | 7.4 | 6.4 | 5.5 | 3.4 | 6.3 | 7 | 3.4 | 7.4 | 5.62 |
| Th | 6.2 | 5.3 | 3.4 | 5.6 | 3.8 | 4.5 | 6.2 | 6.7 | 5.6 | 3.45 | 4.5 | 5.3 | 5.3 | 6.3 | 6.4 | 3.4 | 6.7 | 5.236667 |
| U | 5.09 | 5.47 | 5.85 | 4.5 | 6.23 | 6.23 | 5.66 | 4.34 | 5.63 | 4.56 | 6.23 | 5.23 | 4.23 | 6.11 | 6 | 4.23 | 6.23 | 5.424 |
| V | 34.45 | 71.22 | 82.33 | 109.23 | 87.23 | 134.22 | 109.32 | 98.23 | 112.34 | 24.48 | 52.59 | 80.69 | 108.79 | 136.9 | 165 | 24.48 | 165 | 93.80133 |
| Zn | 25.93 | 16.79 | 7.66 | 65 | 71.2 | 54.3 | 41.23 | 61.2 | 55.3 | 41.2 | 61.23 | 71.2 | 56.3 | 61.2 | 65 | 7.66 | 71.2 | 50.316 |
| Zr | 54.48 | 33.45 | 12.41 | 33.23 | 42.34 | 61.22 | 67.2 | 71.23 | 112.2 | 90.23 | 89.23 | 71.23 | 81.22 | 98.23 | 192 | 12.41 | 192 | 73.99333 |
| La | 21.23 | 23.23 | 19.23 | 21.23 | 19.23 | 21.23 | 18.23 | 17.23 | 21.23 | 22.23 | 28.23 | 21.23 | 19.23 | 10.23 | 30.3 | 10.23 | 30.3 | 20.90133 |
| Ce | 22.23 | 23.44 | 20.12 | 43.23 | 41.23 | 38.23 | 31.23 | 29.23 | 20.23 | 31.23 | 28.23 | 21.23 | 42.12 | 31.24 | 63 | 20.12 | 63 | 32.41467 |

| | | | | | | | | | | | | | | | | | | |
|---|---|---|---|---|---|---|---|---|---|---|---|---|---|---|---|---|---|---|
| Al | 18.3 | 21.23 | 33.2 | 21.22 | 22.23 | 21.23 | 23.6 | 21.78 | 10.1 | 21.23 | 33.2 | 21.22 | 22.23 | 21.23 | 23.6 | 10.1 | 33.2 | 22.37333 |
| Ti | 2.22 | 4.33 | 4.23 | 5.44 | 4.23 | 4.33 | 5.55 | 4.22 | 1.4 | 4.33 | 4.23 | 5.44 | 4.23 | 4.33 | 5.55 | 1.4 | 5.55 | 4.270667 |
| Na | 2.34 | 4.22 | 5.66 | 2.34 | 6.33 | 7.23 | 7.43 | 5.21 | 0.3 | 4.22 | 5.66 | 2.34 | 6.33 | 7.23 | 7.43 | 0.3 | 7.43 | 4.951333 |
| Ca | 4.25 | 5.33 | 8.23 | 4.2 | 5.55 | 4.33 | 4.11 | 6.3 | 2.6 | 5.33 | 8.23 | 4.2 | 5.55 | 4.33 | 4.11 | 2.6 | 8.23 | 5.11 |
| K | 1.5 | 1.8 | 1.34 | 2.33 | 3.34 | 3.23 | 1.5 | 4.22 | 1.5 | 1.8 | 1.34 | 2.33 | 3.34 | 3.23 | 1.5 | 1.34 | 4.22 | 2.286667 |
| Li | 6.04 | 5.66 | 7.87 | 9.876 | 12.65 | 21.56 | 31.65 | 12.54 | 10.65 | 12.56 | 16.67 | 18.77 | 21.67 | 22.43 | 11.23 | 5.66 | 31.65 | 14.7884 |
| Fe | 7.86 | 7.84 | 10.23 | 12.34 | 9.22 | 10.23 | 3.4 | 3.12 | 3.4 | 7.84 | 10.23 | 12.34 | 9.22 | 10.23 | 3.4 | 3.12 | 12.34 | 8.06 |
| B | 8.23 | 10.34 | 11.23 | 12.23 | 10.23 | 8.33 | 9.23 | 11.23 | 14.23 | 10.33 | 10.02 | 9.23 | 9.33 | 7.23 | 10.23 | 7.23 | 14.23 | 10.11 |
| Ge | 1.23 | 3.21 | 1.97 | 2.11 | 1.87 | 1.23 | 1.03 | 2.11 | 2.21 | 4.32 | 3.45 | 1.22 | 1.78 | 1.22 | 1.43 | 1.03 | 4.32 | 2.026 |
| | Bet1 | Bet2 | Bet3 | Bet4 | Bet5 | Bet6 | Bet7 | Bet8 | Bet9 | Bet10 | Bet11 | Bet12 | Bet13 | Bet14 | Bet15 | Min | Max | Mean |
| Light Rare Earth Elements ($\mu g\text{-}g^{-1}$) | | | | | | | | | | | | | | | | | | |
| Sc | 3.97 | 2.4 | 0.83 | 0.59 | 1.25 | 1.9 | 2.56 | 3.21 | 3.87 | 5.26 | 6.82 | 8.39 | 9.96 | 11.53 | 13.1 | 0.59 | 13.1 | 5.042667 |
| Sm | 2.85 | 1.74 | 6.2 | 6.3 | 6.1 | 6.2 | 6.3 | 6.7 | 6.1 | 6.3 | 6.4 | 5.9 | 4.5 | 3.4 | 6.4 | 1.74 | 6.7 | 5.426 |

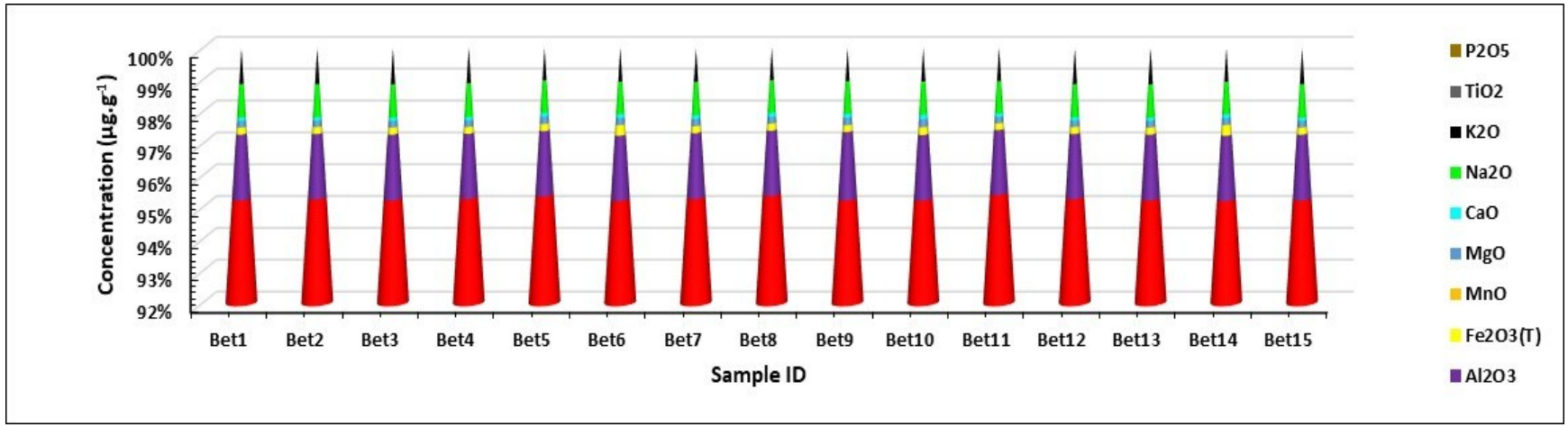


**Fig. 10: Graphical variation in major oxides from the Betem area**

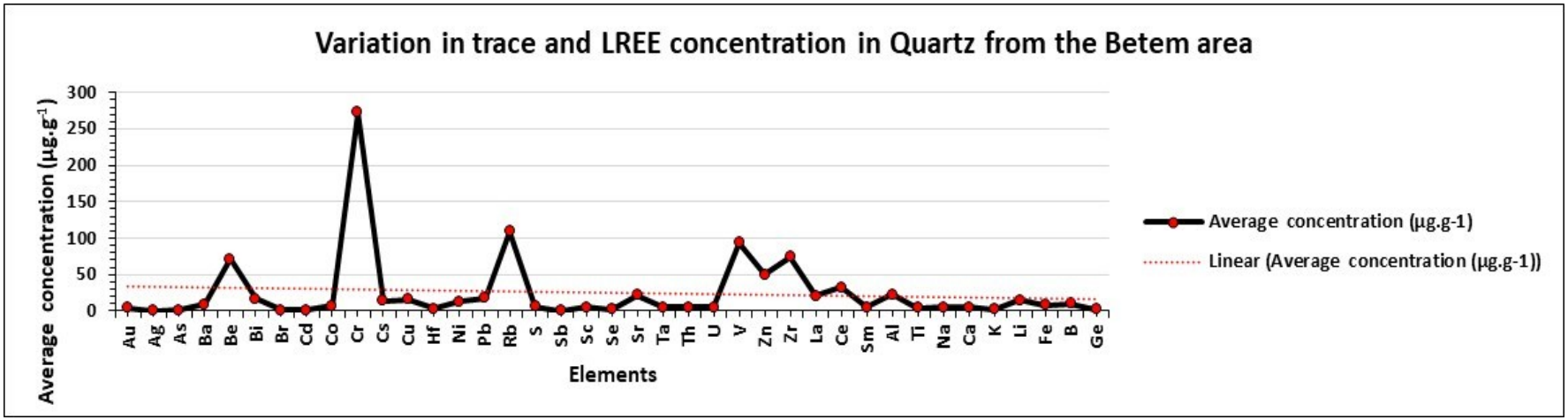


**Fig. 11: Graphical variation in trace elements from the Betem area**

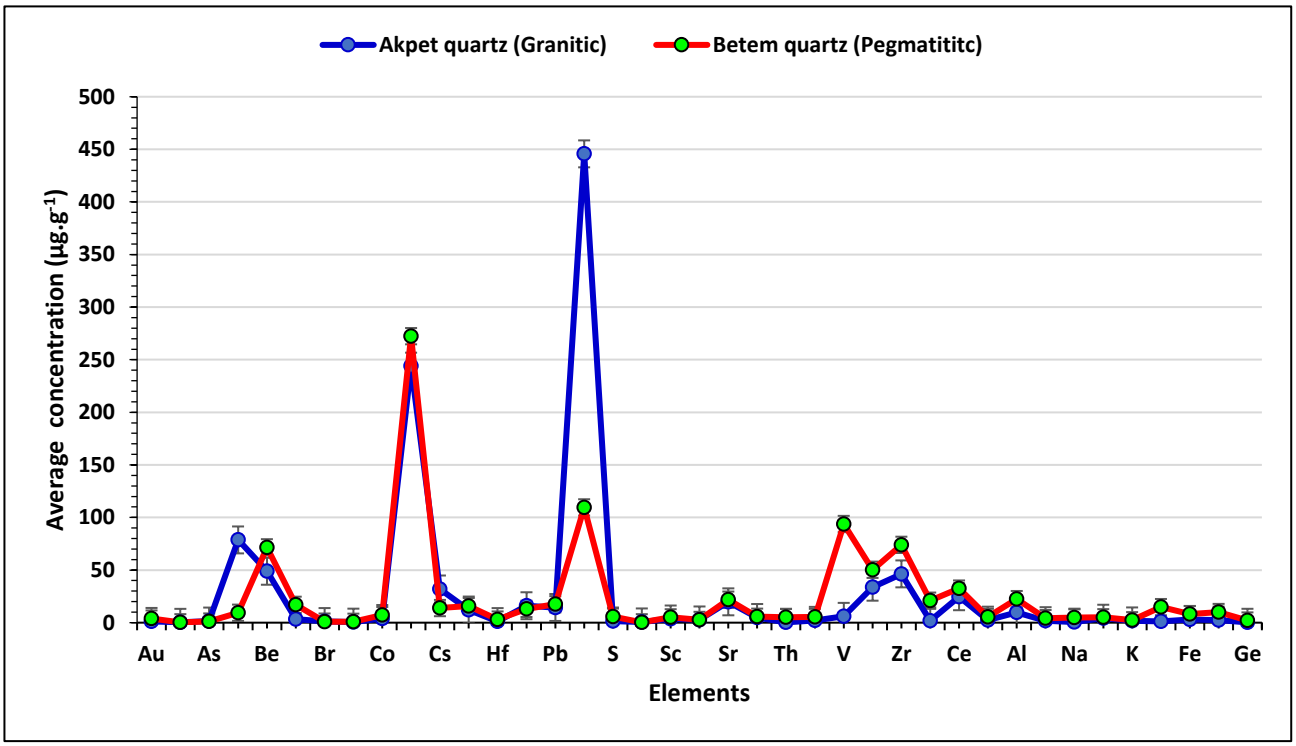


**Fig. 12: Graphical variation in trace elements between Akpet and Betem quartz**

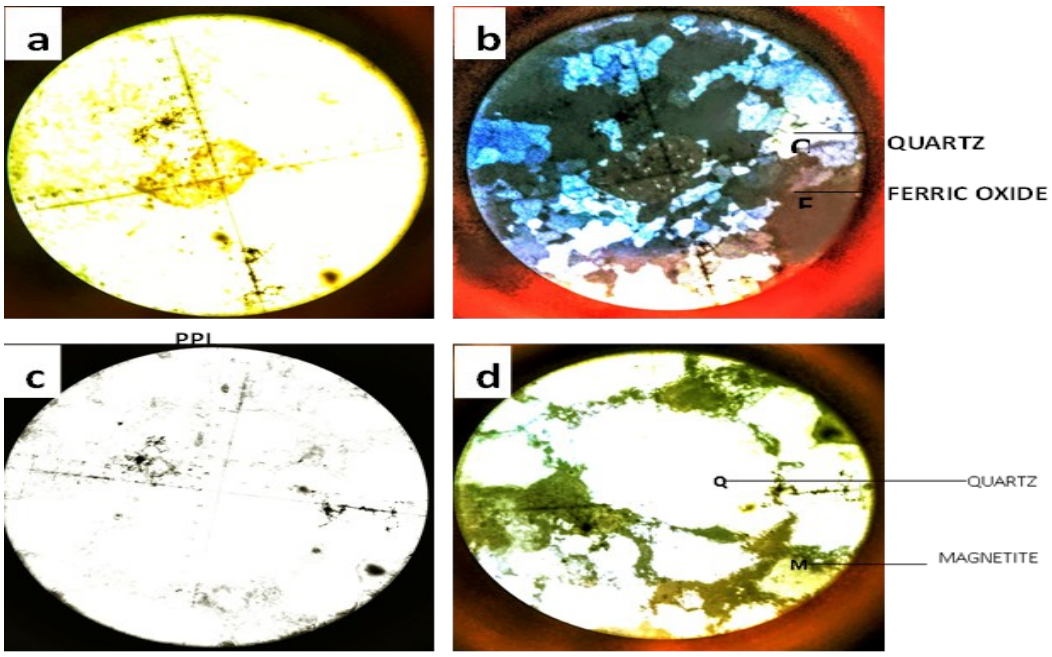


**Fig. 13: Photomicrography of Quartz in plate (a): (MG: x 40, under PPL) (showing the quartz appearing as a dominant, bright, clear, and isotropic mineral with no significant pleochroism observed), (b): (MG: x 40, under CPL) displays first-order interference colors (grey to white), showing a granular texture with interlocking anhedral to subhedral grains typical of quartz; (c): (under PPL) the quartz grains are clear and dominant, appearing isotropic; (d) (under CPL) the quartz displays first-order interference colours, showing interlocking textures, indicative of recrystallized quartz.**

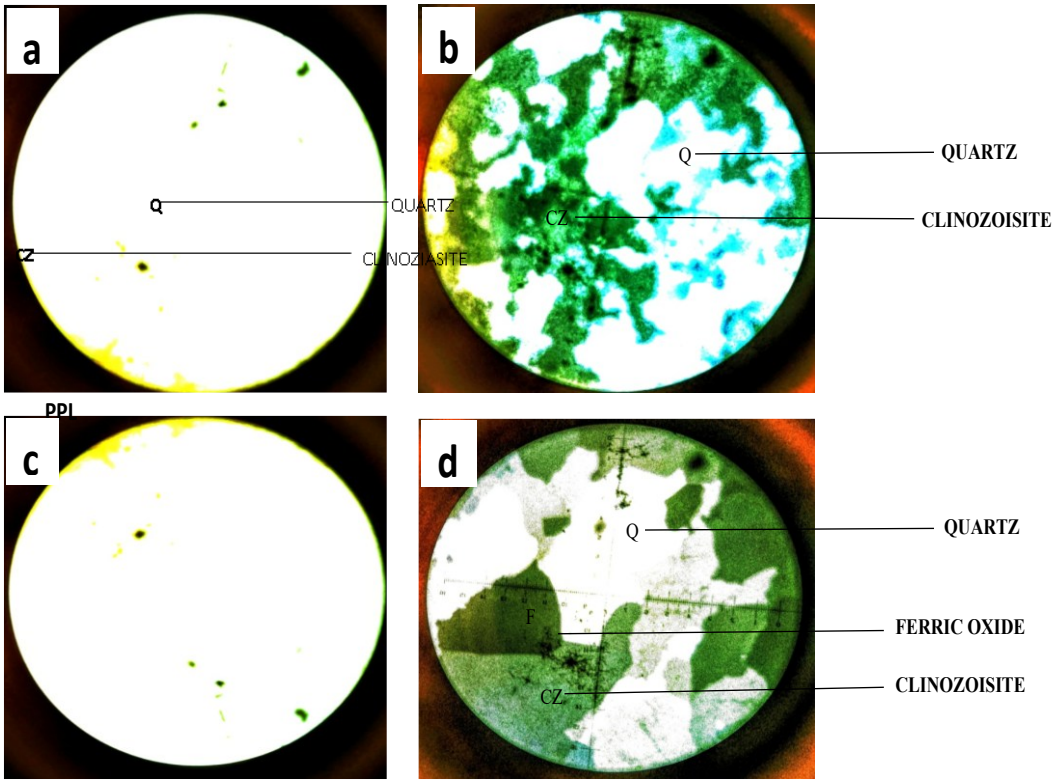


**Fig. 14: Photomicrography of two types of quartz (chalcedony quartz and citrine quartz) from the Betem area: (Chalcedony Quartz), under PPL appears mostly translucent with minimal interference colors due to the microcrystalline nature of chalcedony. b: (Chalcedony Quartz) under CPL; distinct grain boundaries and interlocking mosaic texture become visible. c: (Citrine Quartz under PPL) slightly opaquer with yellowish hues, possibly due to inclusions or intrinsic coloration from ferric components under PPL. d: (Citrine Quartz under CPL), showing a more distinct mineral separation than in chalcedony quartz**

These impurities indicate the presence of feldspars, micas, iron oxides, and possibly clay minerals or carbonate inclusions. Carbon detected in some samples may originate from organic matter or from carbon coating applied during SEM sample preparation. Overall, the impurity levels suggest moderately high-purity quartz. The observed inclusions likely reflect the nature of the host rock, the degree of recrystallization, and fluid activity during metamorphism (Akweteri & Nwachukwu, 2010). Patterns of impurities and inclusions further suggest metasomatic activity or partial melting during metamorphic events, with variability in impurity content reflecting local compositional heterogeneity and differences in metamorphic alteration intensity.

SEM (Scanning Electron Microscope) analyses were conducted at magnifications ranging from 8,000× to 10,000×. For Sample 1A (images A and B) and Sample 1B (images D and E) from the Akpet area, corresponding EDS (Energy Dispersive X-ray Spectroscopy) spectra are presented as Figs 1C and 1F, respectively, providing detailed information on mineral composition, surface morphology, and quartz ($SiO_2$) purity (Fig. 15). Similarly, SEM images at 8,000× and 9,000× magnifications for Sample 2A (images A and B) from the Betem area, along with the EDS spectrum (image C), are shown in Fig. 16.

Table 3 presents the quartz purity results for Akpet and Betem samples, alongside comparisons with regional studies. Aluminium (Al) and titanium (Ti) contents of these samples are plotted in the HPQ (high-purity quartz) field in Fig. 19. The data are categorized into impurity-based fields, including low-purity quartz, medium-purity quartz, and the IOTA standard, providing a benchmark for industrial quality assessment.

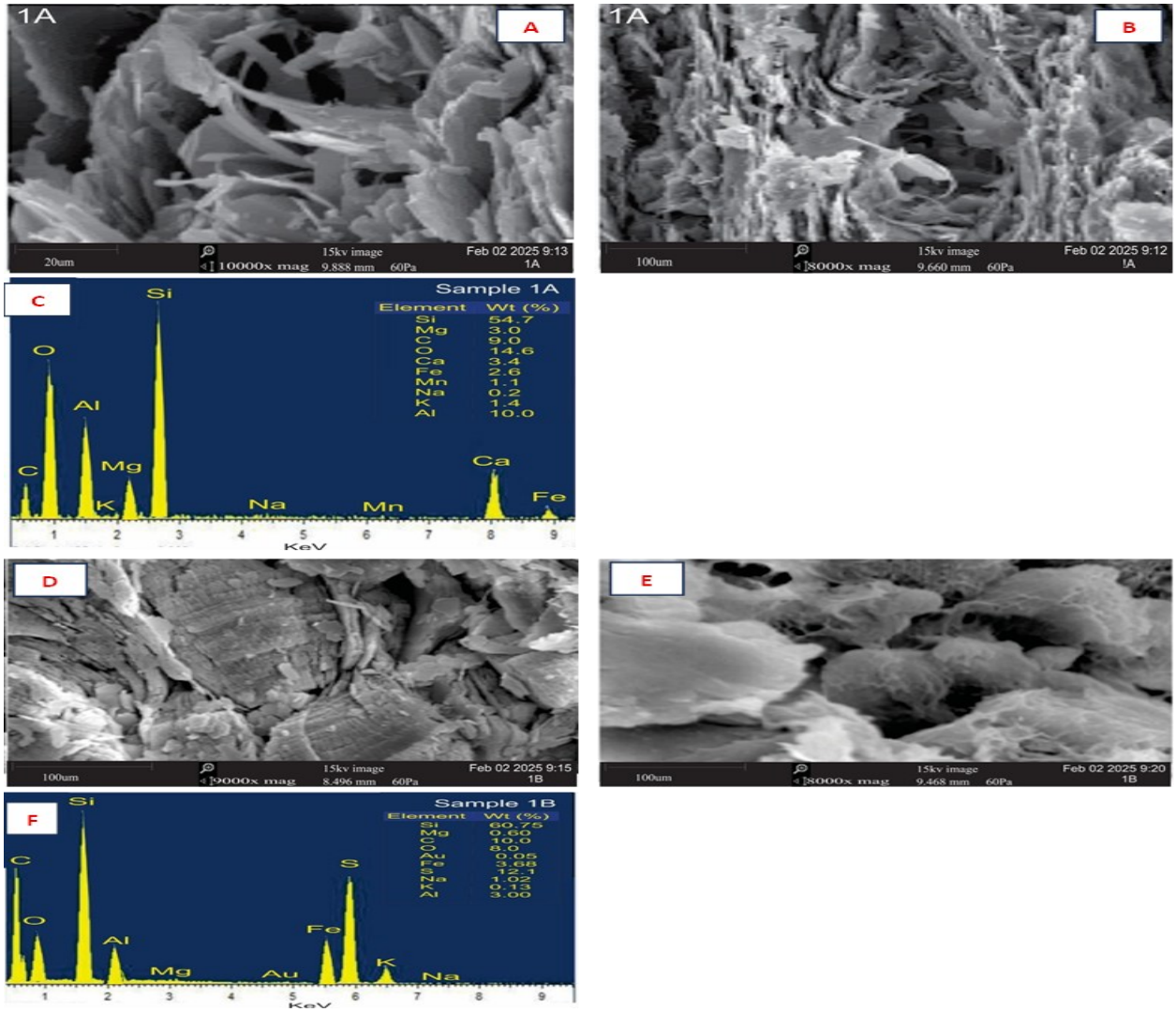


**Fig. 15: Results of SEM (A, B, D, E) images and EDS (C, F) spectrum for Samples A, B, D, E (collected from Akpet area).**

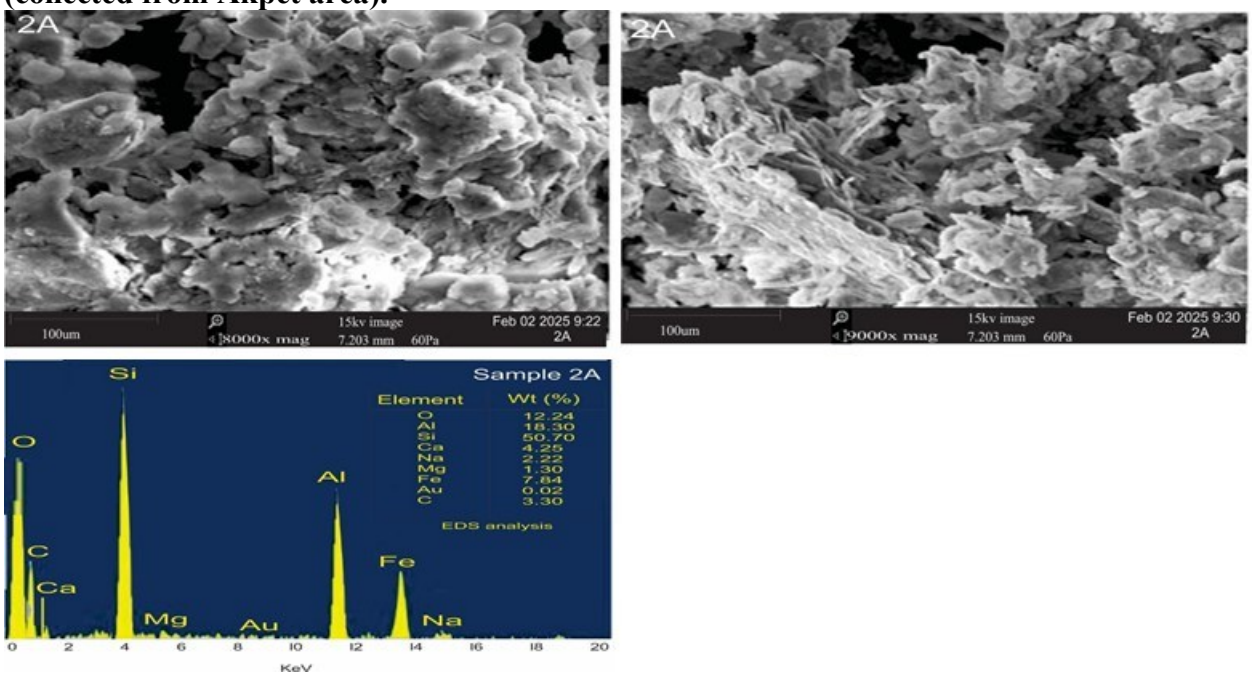


**Fig. 16: Results of SEM (A and B) images and EDS (C) spectrum for Samples A and B (collected from the Betem area)**

**Table 3: Results of the present study compared to other studies showing comparable quartz concentration**

| Location | $SiO_2$ Content / Purity | Accessory Elements | Surface Morphology | Metamorphic Grade | References |
|---|---|---|---|---|---|
| **Betem, SE Nigeria (This study)** | ~50.7 wt% Si (EDS) | Al, Ca, Fe, Na, Mg | Granular, fibrous, irregular | Medium-grade | *This study* |
| **Akpet, SE Nigeria (This study)** | 54.7-60.7 Si (EDS) | Mg, Fe, Na, K, Al | Layered, platy, and angular grains with interlocking and foliated textures | Medium-High grade | *This study* |
| Anambra basin (Nigeria) | 90+(XRF) | Small carbonate blebs, and < 1 % Fe. | Elongated grains, strained | high-grade gneisses | Akweteri & Nwachukwu (2010) |
| Igarra, SW Nigeria | 90–95% $SiO_2$ (XRF) | Al, Fe, Ti | Elongated grains, strained | Amphibolite | Rahaman (1988), Oyinloye (2011) |
| Zungeru-Kaduna, NW Nigeria | ~88–93% $SiO_2$ | Al, K, Fe | Polycrystalline, deformed | Greenschist–Amphibolite | Ajibade & Wright (1981) |
| Ife-Ilesha Schist Belt, SW Nigeria | >90% $SiO_2$ | Fe, Ti, Al | Recrystallized, granoblastic | Medium-grade | Elueze (1981) |
| Scottish Highlands (UK) | ~94% $SiO_2$ | Al, Fe, Na | Undulatory extinction, fibrous | Amphibolite | Yardley (1989) |
| Canadian Shield (Canada) | 85–95% $SiO_2$ | Al, Fe, K | Polygonal, granoblastic | Amphibolite to granulite | Kerrich et al. (1980) |

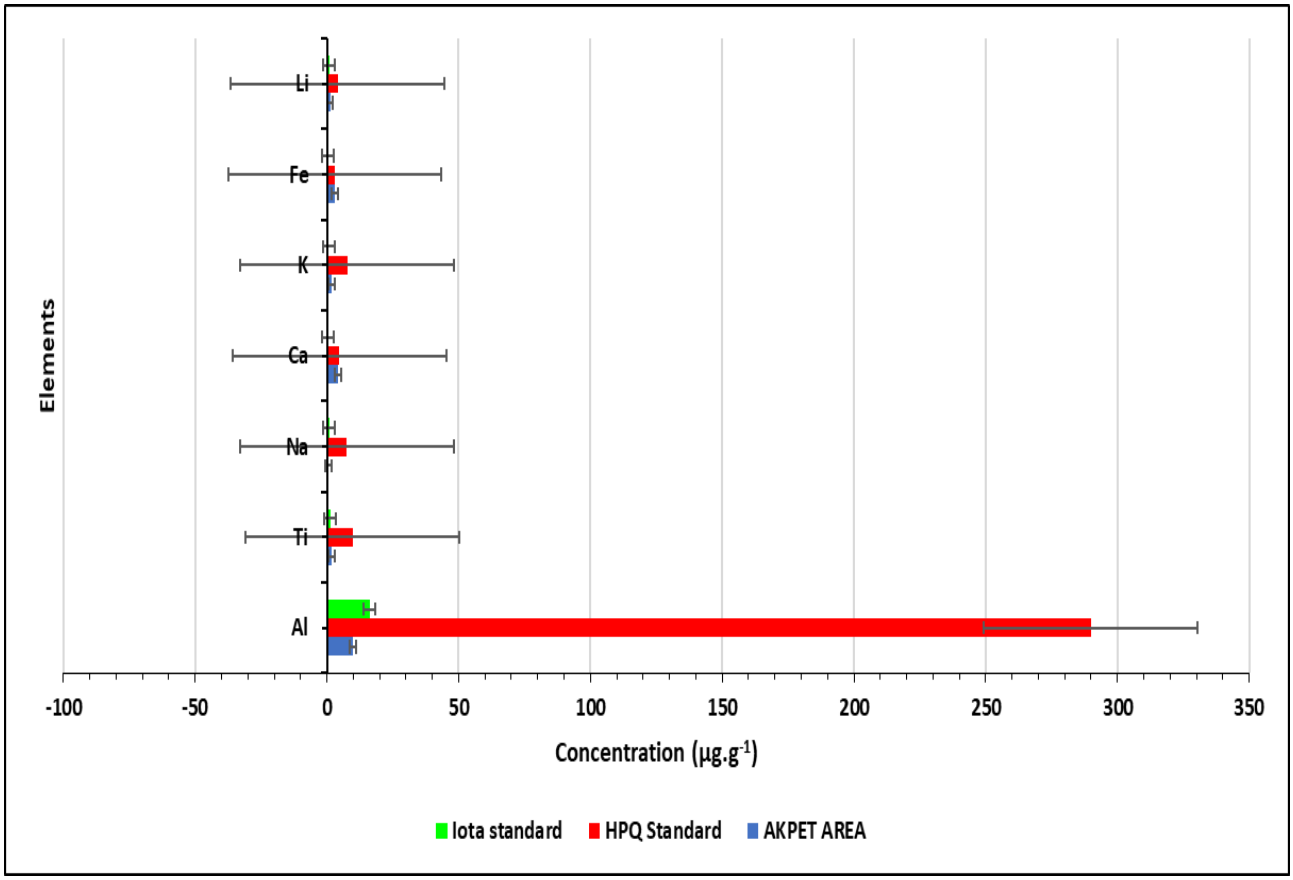


**Fig. 17: Graphical variation of the impurity level of quartz in Akpet compared to IOTA and HPQ standards**

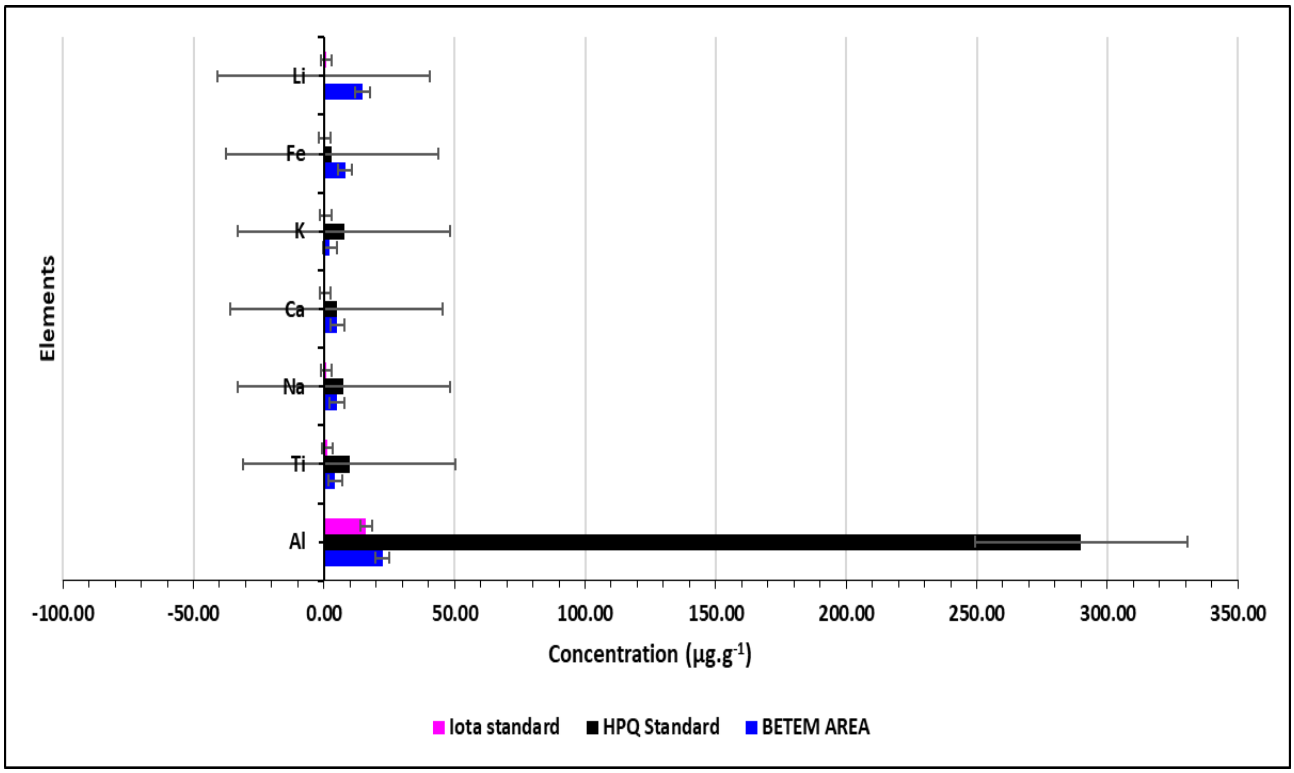


**Fig. 18: Graphical variation of the impurity level of quartz in Betem compared to IOTA and HPQ standards**

Quartz from Akpet generally falls within the medium-purity quartz field, unlike quartz from Betem within the low-purity quartz field.
The red circle represents the IOTA standard, with extremely low impurity levels for both Al and Ti, serving as a benchmark for high-purity quartz.

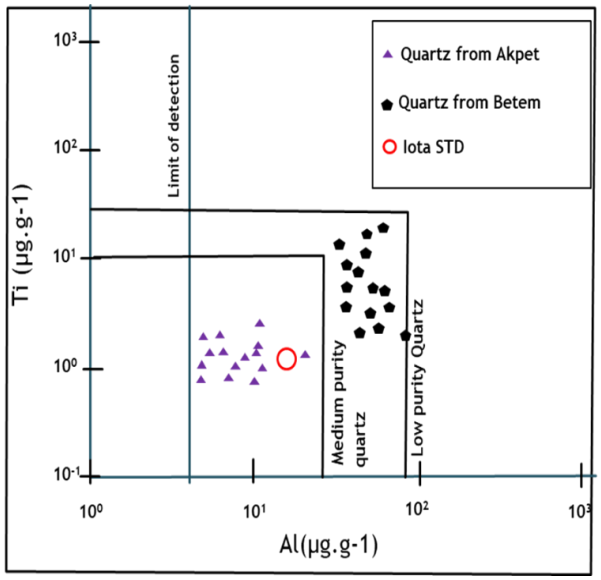


**Fig. 19: Al vs Ti plot of quartz microchemistry from Akpet and Betem. Quartz with Al < 25 µg.g$^{-1}$ and Ti < 10 µg. g$^{-1}$ is considered "high-purity quartz"**

### *3.2.3 Petrogenesis of the Akpet and Betem Quartz Vein Deposit*

The plot in Fig. 20 compares the concentrations of Al and Ti in quartz samples from the Akpet and Betem quartz vein deposits. The data points are plotted against fields associated with different genetic types of quartz deposits: Epithermal, Orogenic Au, and Porphyry-type.
The Akpet quartz falls within the Orogenic Au field (i.e., orogenic gold deposits), which typically forms at medium temperatures (250–400°C) and moderate pressures in structurally controlled settings (Thomas *et al.,* 2011; Müller et al., 2012). The low Ti content in Akpet suggests formation at relatively high fluid pressures and moderate cooling rates, as Ti incorporation into quartz decreases with increasing pressure (Wark & Watson, 2006).
In contrary, quartz from Betem is distributed across the Epithermal field and partially extends into the Orogenic Au field.

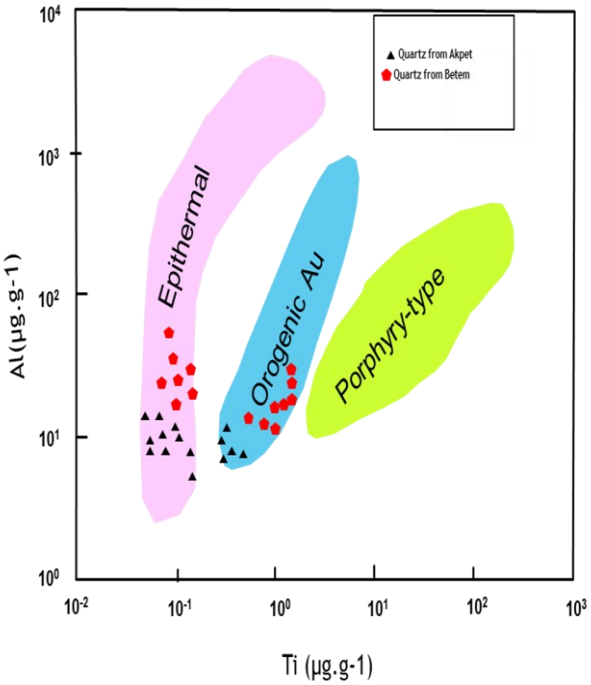


**Fig. 20: Logarithmic Ti versus Al plot of the Akpet and Betem quartz vein deposits (modified after Rusk, 2012)**

### *3.3 Statistical analysis*

### *3.3.1 T-test analysis using one-way ANOVA*

Results of the t-test analysis for Akpet and Betem are presented in Table 4. The t-test compares the trace element compositions of quartz veins from Akpet and Betem to determine whether there is a significant difference between them. The t-test was used to test the null hypothesis that the two quartz veins are not from the same source rock. Hence, significant differences in the trace elements would support the null hypothesis. The P-value, representing the significance threshold (A-value), was set at 0.05. Accordingly, P < 0.05 indicates a significant difference and supports the null hypothesis; however, if P > 0.05, there is no significant difference, failing to support the null hypothesis.
The t-test results showed a significant difference (i.e., P<0.05) for Al, Ti, K, and Li.
However, no significant difference (i.e., P>0.05) in Fe, Ca, and Na. The significant differences observed for Al, Ti, K, and Li support the null hypothesis that the quartz from Akpet and Betem has distinct origins and conclude that the two quartz veins are not from the same source rock; hence, the result supports the hypothesis. In contrast, no significant differences were

observed for Fe, Ca, and Na, indicating that these elements are similar in both quartz veins and do not help distinguish the source rocks.

Relatively increased standard deviation (SD) was observed in Al, Ti, Na, K, and Fe. The variation in SD indicates that it deviates from the mean (Chandrasekaran et al., 2015). This implies that the occurrence of these trace elements in the quartz from the two areas occurred from distinct metamorphic and igneous processes.

### *3.3.2 Principal component analysis (PCA)*

Principal component analysis (using the varimax rotation, at 14 iterations) was used to assess the relationship between bulk rock geochemical properties of major oxides and trace elements in Akpet and Betem, respectively, and to also validate the results from geochemical analysis. Table 5-6 represents the rotated principal component analysis of bulk elemental data from quartz samples in the Akpet and Betem area, respectively. PCA was used in this study to reduce data dimensionality by identifying key components (factors) that explain the majority of the variance in the dataset with respect to quartz purity.

For the Akpet area, a total of 10 principal components (PCs) was extracted with their associated loadings for each variable. High positive or negative loadings were taken at ≥0.5. The first three components (PC1-PC3) explain 65.552% of the total variance in the dataset, indicating that most of the variability in the quartz composition can be summarized by these components, while PC4–PC10 contribute progressively less variance and may capture more specific or subtle geochemical processes. Major oxides like $SiO_2$, $Al_2O_3$, $Fe_2O_3$, MgO, $Na_2O$, $K_2O$, and trace elements (e.g., Pb, Zn, Li) contribute variably to the components, reflecting the influence of source rock, mineral inclusions, and quartz purity. PC1 explains 33.459% of variance, having positive loadings for $SiO_2$ (0.851), $Na_2O$ (0.487), $K_2O$ (0.534), Pb (0.564), Zn (0.434), Se (0.385), and negative loadings for $Fe_2O_3$ (-0.854), $TiO_2$ (-0.553), $Al_2O_3$ (-0.215). PC2 explains 19.585% of variance, showing high positive loadings for MgO (0.575), CaO (0.578), Sr (0.591), Ba (0.541), and negative loadings for As (-0.459), Sb (-0.365), and Cu (-0.385). PC 3 explains 12.508% of variance, showing positive loadings for $Al_2O_3$ (0.372), $TiO_2$ (0.217), Li (0.253), Zr (0.410), and negative loadings for Hf (-0.578), Th (-0.579), and U (-0.431). Other Components (PC4–PC10) explain smaller proportions of the variance and may represent specific processes or localized variations.

The same number of PCS were extracted for the Betem area. PC1 (23.83% variance), recorded a high positive loading for Hf (0.918), Zr (0.874), Nb (0.918), Y (0.874), Th (0.823), Ti (0.738), REEs (La 0.527, Ce 0.553) and high negative loading for Sb (-0.754), Bi (-0.636), Se (-0.612). PC2 (with 17.93% variance) showed high positive loadings for Rb (0.774), $K_2O$ (0.740), Cs (0.621), and negative Loadings for Sr (-0.513) and Ca (-0.514). PC3 (with 10.16% variance) showed high positive loadings for $Fe_2O_3$ (T) (0.476), MnO (0.594), Co (0.519), Cr (0.546), and moderately significant loadings for Ni (0.511), Zn (0.532). PC4 (with 9.45% variance) showed high Positive Loadings for Be (0.555), Ga (0.614), Li (0.529), and B (0.532). PC5 (7.41%) shows moderate loading of U, Mo, and Ba. However, minor variance was explained for PC6–10, likely representing noise or minor geochemical features.

Biplots were generated for the major PCs (PC1 vs PC2 and PC1 vs PC3) in Akpet and Betem, respectively, and presented in Figs 21-22.

$SiO_2$ shows moderate loading on PC2, reflecting that quartz purity (dominated by $SiO_2$) is somewhat independent of other oxides on PC1 but contributes along PC2. $Al_2O_3$ has a significant positive loading on PC2, indicating alumina-bearing phases (e.g., muscovite, feldspar, clays) contribute to variation in quartz purity, likely as inclusions or host rock residues. Samples aligned with positive PC1 likely represent higher $SiO_2$ content, cleaner, and purer quartz, while negative PC1 represents lower $SiO_2$ content and higher impurity levels. The strong positive loading of $SiO_2$ on PC3 suggests that PC3 likely represents quartz purity as a distinct component, independent of PC1 and PC2. Samples high in PC3 are more quartz-rich, with fewer contaminants. $Fe_2O_3$(T) and $Al_2O_3$ have generally negative loadings on PC3, reinforcing that Fe- and Al-bearing phases are anti-correlated with quartz purity. These may originate from mica, clays, feldspar, iron oxides,

or minor accessory minerals incorporated during metamorphism or metasomatism.

**Table 4: Results of the t-test analysis for Akpet and Betem**

| Akpet Quartz | | | | | Betem Quartz | | | | | | |
|---|---|---|---|---|---|---|---|---|---|---|---|
| Element | Min | Max | Mean | SD | Min | Max | Mean | SD | A-value | P-value | Remark |
| Al | 10.3 | 11.3 | 9.786667 | 0.903854 | 10.1 | 33.2 | 22.37333 | 5.431074 | 0.05 | 0.002 | SIG |
| Ti | 1.5 | 3.4 | 1.906667 | 0.69227 | 1.4 | 5.55 | 4.270667 | 1.148828 | 0.05 | 0.006 | SIG |
| Na | 0.4 | 1.2 | 0.492667 | 0.275589 | 0.3 | 7.43 | 4.951333 | 2.247328 | 0.05 | 0.065 | NOT SIG |
| Ca | 6.3 | 8.3 | 4.24 | 1.629549 | 2.6 | 8.23 | 5.11 | 1.541836 | 0.05 | 0.072 | NOT SIG |
| K | 2.1 | 2.2 | 1.673333 | 0.357505 | 1.34 | 4.22 | 2.286667 | 0.944221 | 0.05 | 0.009 | SIG |
| Li | 1.88 | 2 | 1.174667 | 0.61035 | 5.66 | 31.65 | 14.7884 | 7.228676 | 0.05 | 0.0032 | SIG |
| Fe | 2.11 | 4.21 | 3.102 | 0.63032 | 3.12 | 12.34 | 8.06 | 3.249734 | 0.05 | 0.065 | NOT SIG |

***SIG= Significant (P<0.05); NOT SIG= Non-significant (P>0.05); P-value significance threshold (A-value) = 0.05; If P < 0.05, there is a significant difference, supporting the null hypothesis; If P > 0.05, there is no significant difference, failing to support the null hypothesis.***

Increased Reduced Constant

**Table 5: Rotated principal component analysis of bulk elemental data from quartz samples in the Akpet area**

| | Component | | | | | | | | | |
|---|---|---|---|---|---|---|---|---|---|---|
| | 1 | 2 | 3 | 4 | 5 | 6 | 7 | 8 | 9 | 10 |
| $SiO_2$ | 0.015 | 0.432 | -0.128 | 0.349 | 0.062 | -0.025 | 0.588 | -0.3 | -0.29 | -0.273 |
| $Al_2O_3$ | -0.215 | 0.372 | 0.67 | 0.064 | 0.081 | -0.204 | -0.095 | 0.049 | 0.153 | 0.01 |
| $Fe_2O_3$(T) | -0.554 | -0.009 | 0.215 | -0.376 | 0.196 | 0.308 | -0.203 | 0.398 | 0.276 | 0.083 |
| MnO | 0.038 | 0.31 | 0.34 | -0.148 | -0.621 | 0.232 | 0.336 | -0.134 | -0.088 | 0.406 |
| MgO | 0.575 | -0.264 | -0.474 | 0.023 | 0.129 | -0.031 | -0.471 | 0.116 | -0.244 | -0.008 |
| CaO | 0.629 | 0.249 | 0.239 | -0.334 | 0.356 | -0.276 | 0.196 | 0.232 | -0.146 | 0.128 |
| $Na_2O$ | 0.486 | -0.417 | 0.217 | 0.054 | 0.262 | 0.266 | 0.071 | 0.26 | 0.411 | 0.063 |
| $K_2O$ | 0.687 | 0.212 | 0.353 | -0.193 | 0.131 | 0.112 | 0.279 | 0.162 | -0.297 | -0.077 |
| $TiO_2$ | 0.294 | 0.374 | 0.412 | -0.712 | -0.1 | 0.218 | 0.085 | -0.119 | -0.012 | -0.123 |
| $P_2O_5$ | 0.306 | -0.217 | 0.545 | -0.635 | -0.251 | 0.016 | -0.011 | 0.251 | -0.136 | -0.037 |
| Au | -0.776 | 0.605 | 0.115 | -0.013 | 0.11 | 0.01 | 0.014 | 0.027 | -0.005 | 0.004 |
| Ag | 0.869 | -0.4 | 0.235 | 0.116 | 0.066 | 0.017 | -0.047 | -0.066 | -0.02 | 0.046 |
| As | 0.191 | -0.589 | -0.666 | -0.161 | -0.327 | -0.052 | 0.017 | 0.067 | 0.031 | -0.08 |
| Ba | 0.984 | 0.039 | -0.145 | 0 | -0.049 | -0.007 | -0.058 | -0.01 | 0.01 | 0.029 |
| Be | 0.024 | -0.972 | 0.183 | 0.068 | -0.037 | 0.012 | 0.048 | -0.054 | -0.017 | -0.021 |
| Bi | 0.312 | 0.603 | 0.607 | 0.165 | 0.308 | 0.062 | -0.047 | -0.073 | -0.032 | 0.101 |
| Br | -0.965 | 0.161 | -0.154 | -0.082 | -0.045 | -0.022 | 0.047 | 0.058 | 0.007 | -0.051 |
| Cd | -0.686 | 0.587 | 0.359 | 0.059 | 0.199 | 0.025 | 0.008 | -0.008 | -0.017 | 0.024 |
| Co | 0.934 | 0.315 | -0.135 | -0.004 | -0.015 | -0.004 | -0.069 | -0.002 | 0.012 | 0.039 |
| Cr | -0.281 | 0.942 | -0.128 | -0.063 | 0.054 | -0.009 | -0.032 | 0.054 | 0.014 | 0.014 |
| Cs | 0.415 | -0.051 | 0.521 | 0.571 | 0.332 | -0.129 | -0.03 | -0.057 | 0.037 | 0.256 |
| Cu | 0.803 | 0.557 | -0.176 | -0.024 | -0.004 | -0.008 | -0.074 | 0.015 | 0.015 | 0.04 |
| Hf | 0.284 | -0.576 | 0.229 | -0.041 | 0.442 | -0.479 | 0.014 | 0.055 | 0.047 | -0.203 |
| Ni | 0.773 | 0.579 | -0.228 | -0.04 | -0.022 | -0.013 | -0.073 | 0.023 | 0.019 | 0.034 |
| Pb | 0.534 | -0.738 | 0.384 | 0.051 | 0.043 | 0.053 | 0.019 | -0.097 | -0.03 | 0.01 |
| Rb | 0.106 | -0.972 | 0.095 | 0.12 | -0.049 | 0.056 | 0.002 | -0.032 | -0.048 | -0.069 |
| S | 0.584 | 0.39 | 0.508 | -0.168 | -0.271 | 0.155 | 0.143 | -0.049 | -0.013 | -0.203 |
| Sb | 0.83 | -0.545 | -0.053 | 0.029 | -0.077 | -0.005 | -0.02 | -0.034 | 0.006 | 0.004 |
| Sc | 0.895 | 0.385 | -0.196 | -0.023 | -0.03 | -0.01 | -0.07 | 0.01 | 0.016 | 0.034 |
| Se | 0.038 | 0.064 | -0.437 | 0.191 | 0.568 | 0.465 | 0.08 | -0.283 | -0.167 | -0.244 |
| Sr | 0.725 | -0.608 | 0.291 | 0.076 | 0.036 | 0.027 | 0.001 | -0.084 | -0.016 | 0.035 |
| Ta | 0.509 | -0.619 | 0.538 | -0.017 | 0.082 | 0.17 | -0.008 | -0.116 | -0.088 | -0.069 |
| Th | 0.382 | 0.552 | 0.599 | 0.244 | 0.046 | -0.073 | -0.103 | -0.201 | 0.114 | -0.158 |
| U | 0.887 | 0.389 | 0.164 | 0.073 | 0.111 | 0.023 | -0.069 | -0.038 | -0.008 | 0.072 |
| V | -0.314 | -0.254 | 0.072 | 0.356 | -0.353 | 0.184 | -0.199 | -0.195 | -0.329 | 0.565 |
| Zn | 0.979 | 0.008 | -0.173 | -0.007 | -0.063 | -0.009 | -0.056 | -0.007 | 0.012 | 0.025 |
| Zr | 0.88 | 0.415 | -0.199 | -0.025 | -0.029 | -0.01 | -0.071 | 0.011 | 0.016 | 0.035 |
| La | 0.687 | -0.019 | -0.133 | -0.44 | -0.025 | -0.023 | 0.255 | -0.399 | 0.201 | 0.128 |
| Ce | 0.809 | 0.247 | -0.279 | 0.099 | -0.162 | -0.097 | 0.048 | 0.183 | 0.195 | 0.01 |
| Sm | 0.877 | 0.421 | -0.2 | -0.026 | -0.028 | -0.01 | -0.071 | 0.011 | 0.016 | 0.035 |
| Al | -0.051 | -0.045 | -0.026 | 0.585 | -0.412 | -0.275 | 0.487 | -0.006 | 0.342 | -0.091 |
| Ti | 0.094 | -0.258 | -0.34 | -0.14 | 0.375 | -0.345 | 0.533 | 0.351 | -0.221 | 0.125 |
| Na | 0.15 | -0.055 | -0.536 | -0.033 | 0.317 | 0.204 | 0.338 | -0.088 | 0.527 | 0.326 |
| Ca | 0.232 | 0.325 | 0.033 | 0.609 | -0.17 | 0.471 | -0.259 | 0.265 | 0.073 | -0.221 |
| K | 0.578 | 0.163 | 0.143 | 0.554 | -0.36 | -0.106 | 0.097 | 0.313 | 0.007 | -0.19 |
| Li | -0.259 | -0.253 | 0.784 | 0.063 | 0.253 | 0.303 | 0.083 | -0.133 | 0.153 | 0.011 |
| Fe | 0.218 | -0.109 | -0.539 | -0.216 | 0.135 | 0.664 | 0.017 | -0.229 | 0.057 | -0.188 |
| B | 0.077 | 0.063 | -0.215 | 0.37 | 0.336 | 0.518 | 0.284 | 0.412 | -0.27 | 0.245 |
| Ge | 0.029 | -0.247 | 0.27 | -0.037 | -0.388 | 0.465 | 0.285 | 0.359 | -0.003 | -0.148 |
| Total | 16.395 | 9.597 | 6.143 | 3.482 | 2.813 | 2.467 | 1.94 | 1.594 | 1.345 | 1.237 |
| % of Variance | 33.459 | 19.586 | 12.537 | 7.107 | 5.741 | 5.035 | 3.959 | 3.252 | 2.745 | 2.525 |

| | | | | | | | | | | |
|---|---|---|---|---|---|---|---|---|---|---|
| Cumulative % | 33.459 | 53.045 | 65.582 | 72.689 | 78.429 | 83.464 | 87.423 | 90.675 | 93.42 | 95.945 |

**Table 6: Rotated principal component analysis of bulk elemental data from quartz samples in the Betem area**

| | Component | | | | | | | | | |
|---|---|---|---|---|---|---|---|---|---|---|
| | 1 | 2 | 3 | 4 | 5 | 6 | 7 | 8 | 9 | 10 |
| $SiO_2$ | -0.38 | 0.142 | 0.007 | -0.388 | 0.145 | -0.501 | 0.333 | 0.324 | 0.307 | 0.084 |
| $Al_2O_3$ | -0.349 | 0.187 | -0.486 | -0.515 | 0.183 | 0.086 | 0.131 | 0.116 | -0.335 | 0.34 |
| $Fe_2O_3$(T) | 0.19 | 0.275 | 0.477 | -0.216 | -0.571 | 0.255 | -0.29 | 0.067 | -0.107 | 0.059 |
| MnO | -0.298 | 0.079 | -0.264 | 0.572 | 0.022 | 0.181 | -0.373 | 0.346 | 0.381 | 0.082 |
| MgO | -0.585 | 0.393 | 0.079 | -0.173 | 0.015 | 0.511 | -0.065 | 0.226 | 0.041 | 0.145 |
| CaO | -0.599 | 0.449 | 0.257 | -0.033 | -0.15 | 0.361 | -0.261 | -0.129 | 0.269 | 0.17 |
| $Na_2O$ | 0.427 | -0.442 | -0.421 | -0.073 | 0.362 | -0.138 | -0.059 | 0.353 | 0.272 | 0.006 |
| $K_2O$ | 0.548 | -0.098 | 0.029 | 0.076 | -0.398 | -0.276 | 0.402 | 0.443 | -0.113 | 0.115 |
| $TiO_2$ | -0.304 | 0.469 | -0.017 | -0.14 | -0.362 | 0.352 | -0.053 | 0.572 | 0.035 | 0.203 |
| $P_2O_5$ | 0.575 | -0.532 | -0.408 | 0.093 | 0.266 | -0.228 | -0.166 | 0.114 | 0.019 | 0.094 |
| Au | -0.026 | 0.553 | 0.604 | 0.09 | 0.504 | 0.005 | 0.046 | 0.025 | -0.09 | 0.193 |
| Ag | 0.775 | -0.603 | 0.048 | -0.086 | -0.048 | 0.104 | -0.089 | -0.016 | -0.004 | 0.047 |
| As | -0.833 | 0.458 | -0.175 | 0.061 | -0.075 | -0.152 | 0.096 | 0.046 | 0.042 | -0.109 |
| Ba | -0.003 | -0.674 | -0.514 | -0.118 | -0.456 | 0.009 | -0.04 | -0.015 | 0.091 | -0.183 |
| Be | 0.765 | 0.566 | -0.213 | 0.135 | -0.058 | 0.023 | -0.075 | -0.071 | -0.066 | 0.082 |
| Bi | 0.393 | -0.818 | 0.324 | -0.148 | 0.123 | 0.145 | -0.05 | -0.004 | -0.005 | 0.065 |
| Br | 0.751 | 0.596 | -0.181 | 0.14 | -0.03 | 0.021 | -0.072 | -0.068 | -0.07 | 0.087 |
| Cd | 0.417 | -0.806 | 0.323 | -0.144 | 0.124 | 0.144 | -0.048 | -0.006 | -0.007 | 0.069 |
| Co | 0.804 | 0.483 | -0.26 | 0.121 | -0.102 | 0.03 | -0.084 | -0.075 | -0.059 | 0.068 |
| Cr | 0.382 | -0.874 | 0.195 | -0.156 | 0.024 | 0.136 | -0.056 | -0.008 | 0.011 | 0.027 |
| Cs | 0.823 | -0.207 | -0.034 | -0.395 | 0.146 | 0.003 | 0.032 | -0.097 | -0.03 | 0.261 |
| Cu | 0.871 | 0.358 | -0.247 | 0.099 | -0.109 | 0.049 | -0.093 | -0.078 | -0.057 | 0.069 |
| Hf | 0.723 | 0.155 | 0.046 | 0.513 | -0.024 | -0.137 | 0.059 | 0.032 | 0.328 | 0.17 |
| Ni | 0.918 | 0.091 | -0.289 | 0.051 | -0.175 | 0.074 | -0.108 | -0.08 | -0.039 | 0.043 |
| Pb | 0 | 0.516 | -0.316 | 0.546 | -0.044 | -0.376 | -0.094 | 0.126 | -0.323 | -0.012 |
| Rb | 0.718 | 0.391 | -0.115 | -0.089 | -0.125 | 0.26 | 0.292 | 0.056 | 0.166 | 0.019 |
| S | 0.284 | 0.141 | 0.024 | 0.044 | 0.496 | -0.212 | -0.448 | 0.538 | -0.209 | -0.239 |
| Sb | -0.025 | -0.202 | 0.021 | -0.07 | -0.254 | 0.833 | -0.26 | 0.151 | 0.127 | -0.28 |
| Sc | 0.612 | 0.659 | -0.361 | 0.15 | -0.152 | -0.017 | -0.063 | -0.068 | -0.048 | 0.033 |
| Se | -0.157 | 0.023 | -0.159 | -0.363 | -0.532 | -0.233 | 0.412 | -0.157 | 0.06 | -0.36 |
| Sr | 0.563 | -0.019 | 0.011 | -0.387 | 0.422 | 0.397 | 0.156 | 0.238 | -0.007 | -0.097 |
| Ta | -0.073 | 0.087 | -0.522 | 0.256 | 0.085 | 0.524 | 0.12 | -0.207 | -0.043 | 0.127 |
| Th | 0.283 | 0.237 | -0.311 | -0.575 | -0.122 | -0.432 | 0.038 | -0.247 | 0.332 | -0.105 |
| U | 0.2 | 0.055 | 0.258 | -0.165 | -0.212 | 0.436 | 0.367 | 0.132 | -0.52 | -0.167 |
| V | 0.525 | 0.376 | 0.311 | -0.579 | 0.226 | -0.001 | 0.025 | -0.071 | -0.054 | 0.165 |
| Zn | 0.112 | 0.656 | 0.22 | -0.06 | 0.343 | -0.138 | -0.283 | -0.293 | -0.146 | -0.39 |
| Zr | 0.321 | 0.757 | -0.397 | -0.153 | 0.114 | 0.281 | 0.142 | -0.096 | 0.058 | -0.1 |
| La | 0.127 | -0.036 | -0.392 | 0.249 | 0.432 | 0.296 | 0.365 | 0.051 | 0.001 | -0.486 |
| Ce | 0.582 | 0.284 | 0.214 | -0.158 | 0.388 | 0.336 | -0.041 | -0.159 | 0.275 | -0.239 |
| Sm | -0.244 | 0.4 | 0.369 | 0.09 | 0.606 | 0.083 | 0.297 | 0.001 | -0.081 | -0.09 |
| Al | 0.322 | -0.195 | 0.367 | 0.617 | -0.045 | 0.012 | 0.568 | -0.022 | -0.043 | 0.014 |
| Ti | 0.523 | 0.111 | 0.448 | 0.301 | 0.32 | -0.13 | 0.053 | 0.258 | 0.405 | -0.109 |
| Na | 0.482 | 0.248 | 0.605 | 0.047 | -0.278 | 0.197 | 0.328 | 0.014 | 0.226 | 0.023 |
| Ca | -0.001 | -0.264 | 0.28 | 0.703 | -0.109 | -0.014 | 0.47 | -0.296 | -0.063 | 0.138 |
| K | 0.007 | 0.235 | 0.556 | -0.073 | -0.118 | -0.265 | -0.488 | -0.475 | 0.144 | 0.038 |
| Li | 0.103 | 0.583 | 0.471 | -0.12 | -0.225 | -0.347 | 0.119 | 0.426 | 0.038 | -0.083 |
| Fe | 0.221 | -0.319 | 0.294 | 0.497 | -0.061 | -0.107 | -0.443 | 0.133 | -0.412 | -0.122 |
| B | -0.468 | -0.094 | -0.217 | -0.123 | 0.715 | 0.052 | 0.156 | -0.214 | -0.091 | 0.282 |
| Ge | -0.457 | -0.033 | -0.2 | 0.63 | 0.096 | 0.338 | 0.054 | -0.111 | 0.222 | 0.084 |
| Total | 11.703 | 8.787 | 4.981 | 4.589 | 4.023 | 3.633 | 2.854 | 2.317 | 1.829 | 1.427 |
| % of Variance | 23.883 | 17.933 | 10.166 | 9.365 | 8.211 | 7.415 | 5.825 | 4.728 | 3.733 | 2.912 |

ZZ

| | | | | | | | | | | |
|---|---|---|---|---|---|---|---|---|---|---|
| Cumulative % | 23.883 | 41.816 | 51.982 | 61.347 | 69.557 | 76.972 | 82.797 | 87.525 | 91.258 | 94.17 |

The association of trace elements (Ba, Cu, Zn, Na, K, Rb, Sr) with PC1 (rather than PC2 or PC3) suggests they are largely independent of quartz purity and likely reflect alteration or host rock contribution.

For Betem, the first plot (PC1 vs PC2), PC1 (horizontal, ~y-axis~ *x-axis*) is dominated by REE-Zr-Hf-Ti-Th association, while PC2 (vertical, ~x-axis~ *y-axis*) is dominated by Rb-$K_2O$-Cs (positive) vs. Ca-Sr (negative). For the second plot (PC1 vs PC3), PC1 has an enrichment of REE-Zr-Hf, while PC3 reflects base metals (Mn, Zn, Co, Cr, Ni).

### 3.4 Discussion

#### *3.4.1 Genetic Implications for the Akpet and Betem Quartz Vein Deposits*

Quartz from Akpet likely formed during crustal deformation events, such as regional metamorphism, shear zone activity, or tectonic compression. Quartz in orogenic deposits is often associated with gold mineralization and may contain trace metals indicative of hydrothermal fluids, forming in shear zones, faults, or veins under compressional regimes. The low Ti and moderate Al observed in the Akpet quartz further supports its classification as orogenic. On the contrary, Betem quartz is characteristic of epithermal deposits, suggesting formation at low temperatures (<300°C) and shallow crustal environments (typically <1.5 km) under magmatic-hydrothermal systems, where fluids are enriched in metallic elements and interact with host rocks (Garba, 2003). Although *epithermal deposits* are less common in the Nigerian Basement Complex, a study by Obaje (2009) observed epithermal deposits in areas associated with shallow magmatic intrusions. These deposits form at lower pressures and temperatures compared to orogenic deposits, allowing for greater incorporation of Ti into quartz, exhibiting textures such as colloform banding, open-space filling, and vuggy quartz.

In terms of texture, the Akpet quartz is characterized by recrystallized quartz grains, deformation bands, locally strained grains, and vein-type infillings in shear zones with evidence of multiple fluid flow events. Given the texture, it is inferred that the quartz vein was produced by hydrothermal conditions (from orogenic fluids) with relatively stable flow conditions (Goldfarb et al., 2001). Orogenic fluids are typically $CO_2$-rich, with moderate salinity, sourced from metamorphic devolatilization or deep crustal processes and can transport trace metals. Such a fluid is enriched in Fe, Ca, Na, Al, and minor Ti, as observed in the quartz microchemistry. Given limited secondary hydrothermal overprinting, it is inferred that the impurity-bearing quartz results from the original metal-rich metamorphic fluid rather than secondary contamination by an external fluid (Rusk et al., 2008; Rusk, 2012).

Trace element trends observed in Akpet quartz are similar to those in orogenic belts globally, such as the Canadian Shield and Western Australia. These studies highlight the role of compressional tectonics and high-pressure fluids in quartz formation. The Betem quartzes are comparable to deposits in volcanic arcs like the Andes and Japan, where high Ti and Al quartz forms at shallow depths. The Betem quartz's overlap with the *orogenic Au field* suggests a transitional environment, similar to hybrid systems reported in the Tibetan Plateau.

Based on genetic evolution and deposit *formation*, the Akpet Quartz likely formed during the Pan-African orogeny (600–550 Ma), characterized by crustal thickening and regional metamorphism (Obaje, 2009). The fluids derived from metamorphic devolatilization may have infiltrated shear zones, precipitating quartz and associated minerals and potentially trace metals under high-pressure conditions.

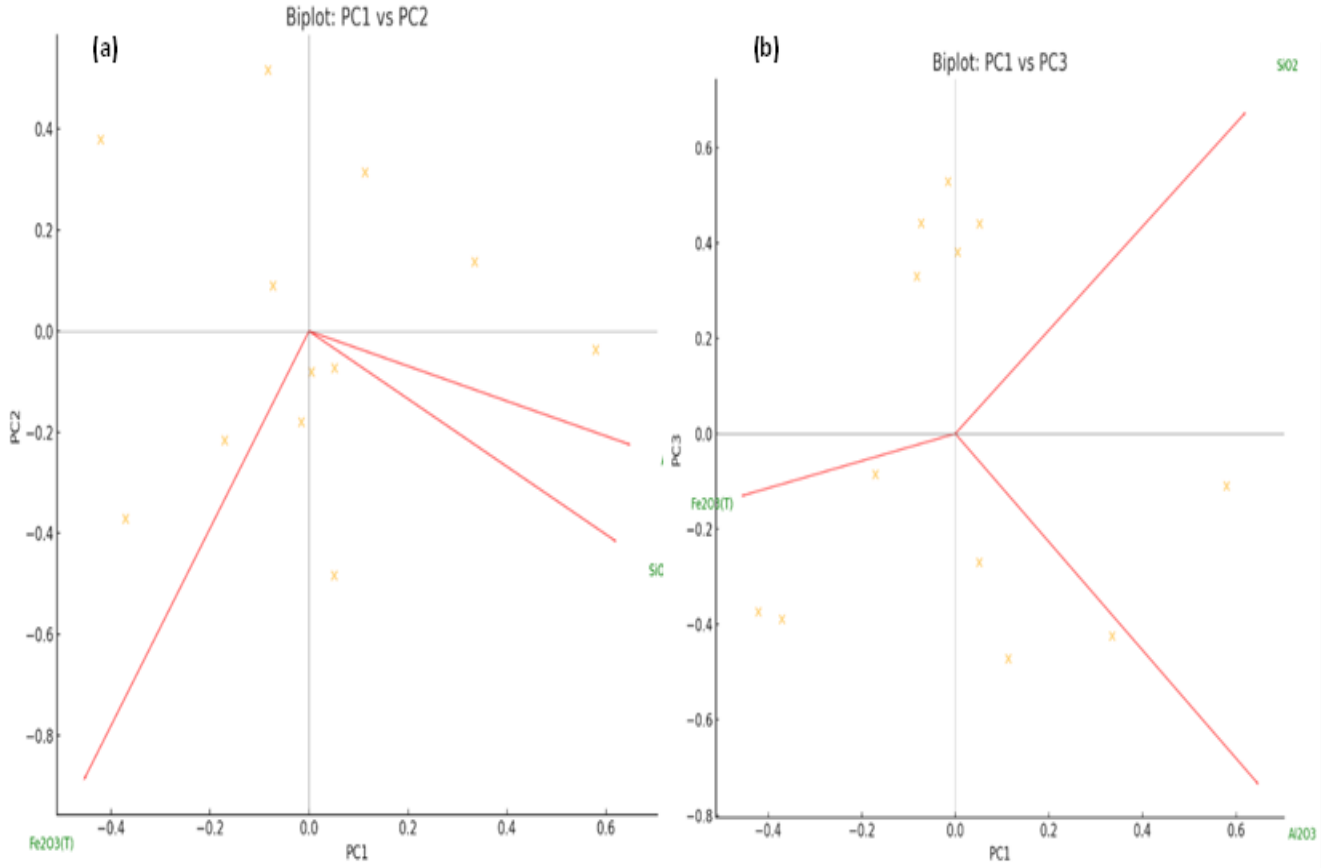


**Fig. 21: Biplots generated for the major PCs (PC1 vs PC2 and PC1 vs PC3) in Akpet area**

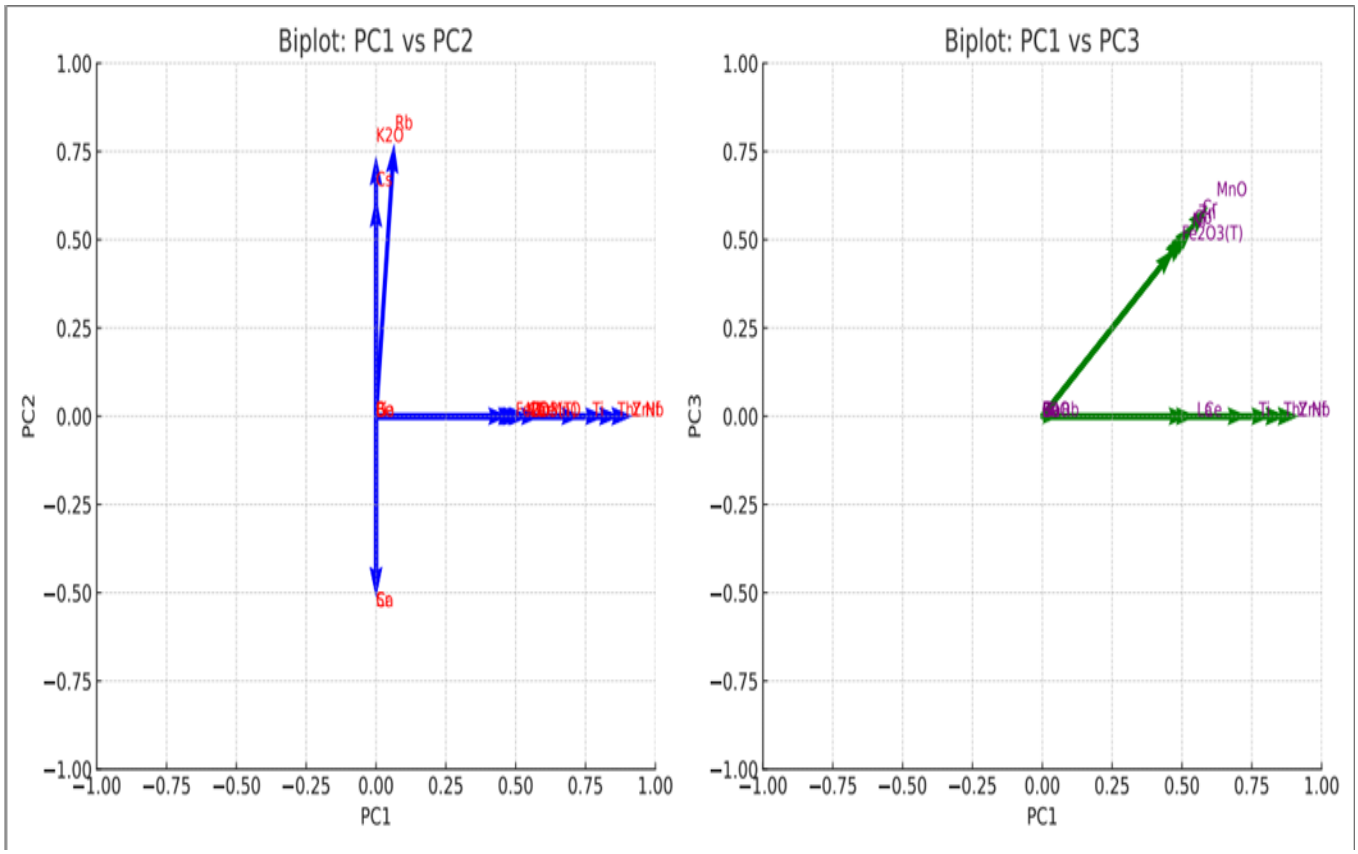


**Fig. 22: Biplots generated for the major PCs (PC1 vs PC2 and PC1 vs PC3) in Betem area**

Orogenic gold systems are globally significant for gold mineralization, making the Akpet quartz veins potentially strategic targets for gold exploration and associated precious metals. In contrast, the Betem Quartz likely formed in a shallow magmatic-hydrothermal system, potentially linked to post-orogenic magmatism or extensional tectonics, correlating with the findings of Müller et al. (2012 a & b). The low-pressure, low-temperature fluids interacted extensively with host rocks, precipitating quartz with high Ti and Al concentrations. Epithermal systems are known for base and precious metal deposits (Lehmann and Romano, 2005), highlighting the potential of Betem quartz veins for silver and base metal exploration.

### *3.4.2 Major oxide and trace element association for source rock identification*

#### *3.4.2.1 Assessment of trace element compositions in quartz veins from Akpet and Betem*

Results from t-test analysis using the one-way ANOVA parametric analysis are presented in Table 4. The t-test results compare the trace element composition of quartz veins from Akpet and Betem, highlighting significant geochemical differences. The results showed significant differences for Al, Ti, and K, indicating that quartz from Akpet and Betem likely originated from distinct source rocks. In contrast, no significant difference was observed for Fe, Ca, and Na. The higher variability in Al content in Betem quartz (mean = 22.73 $\mu g\text{-}g^{-1}$) could indicate a more evolved pegmatitic system, where Al is concentrated due to fractional crystallization. Conversely, Akpet quartz (mean = 9.79 $\mu g\text{-}g^{-1}$) reflects a less evolved granitic source. Aluminium (Al) is typically incorporated into quartz during crystallization from magma or hydrothermal fluids (Götze et al., 2004). The higher Al content in Betem quartz suggests that the pegmatitic source rock was richer in Al-bearing minerals (feldspars, micas) or that the crystallizing fluids were more Al-enriched. In contrast, the lower Al content in Akpet quartz reflects the less evolved nature of the granitic source, where Al concentrations in the melt or fluids remained relatively low.

Titanium (Ti) incorporation into quartz is temperature-dependent and indicates the thermal conditions of quartz crystallization (Wark & Watson, 2006). The higher Ti content in Betem quartz (mean = 4.27 $\mu g\text{-}g^{-1}$) suggests crystallization at higher temperatures compared to Akpet quartz (mean = 1.90 $\mu g\text{-}g^{-1}$). This difference aligns with the fact that pegmatites often form at higher temperatures than granitic intrusions, explaining the elevated Ti in Betem quartz. Moreover, Titanium is sourced from Ti-bearing minerals such as biotite, rutile, and ilmenite in the parent rock (Thomas et al., 2011). The higher Ti content in Betem quartz further indicates a pegmatitic source or more Ti-enriched magmatic fluids, while the lower Ti content in Akpet quartz suggests the granitic source rock was less Ti-enriched or crystallization conditions limited Ti incorporation.

Potassium is a key component of K-feldspar and micas, which are more abundant in evolved granitic and pegmatitic systems. The higher K content in Betem quartz (mean = 2.28 $\mu g\text{-}g^{-1}$) indicates a more potassium-enriched environment, typical of pegmatites. The difference in K content supports a pegmatitic origin for Betem quartz, as pegmatites often form from highly fractionated magmas enriched in alkali elements like K (London, 2008).

Lithium (Li) is often associated with late-stage magmatic fluids enriched in pegmatitic systems. The significantly higher Li content in Betem quartz (mean = 14.78 $\mu g\text{-}g^{-1}$) confirms a strong pegmatitic signature, reflecting the high degree of magmatic differentiation and fluid-rock interaction characteristic of pegmatitic systems (Černý & Ercit, 2005). Akpet quartz (mean = 1.17 $\mu g\text{-}g^{-1}$) likely formed in a less evolved granitic environment.

No significant difference was observed in Na and Fe between Akpet and Betem (Table 4). Sodium (Na) is a major component of plagioclase feldspar, and its presence in quartz usually arises from fluid inclusions or trace contamination during crystallization. The similarity in Na content suggests both quartz veins interacted with fluids of similar sodium composition. Calcium (Ca), often associated with carbonate minerals or feldspars, showed consistent levels in both sites, indicating similar fluid chemistry during quartz formation. Iron (Fe) is typically related to fluid inclusions or trace contamination, and the lack of significant

difference indicates similar Fe concentrations in both systems.

#### *3.4.2.2 Relationship between bulk rock geochemical properties of major oxides and trace elements in Akpet and Betem*

High $SiO_2$ loading (PC1) observed in Akpet indicates quartz purity, reflecting significant silica enrichment. Negative $Fe_2O_3$ and $TiO_2$ loadings imply that iron and titanium oxides, often found in mineral inclusions, negatively correlate with quartz purity. This suggests quartz with fewer inclusions is chemically purer.

Positive loadings for $Na_2O$ and $K_2O$ reflect alkali enrichment, possibly related to interaction with hydrothermal fluids or feldspar inclusions (London, 2008). High positive loadings for Pb and Zn indicate potential mineralization linked to sulfide or hydrothermal processes (Götze et al., 2004; Müller et al., 2012). The contributions of PC2 and PC3 highlight the role of feldspar, mica, and carbonate inclusions in quartz, indicating the host rock likely contains granitic or pegmatitic minerals. Trace elements like Li, Zr, and Sr reflect **evolved source rock composition**, suggesting quartz formed in highly fractionated magmatic systems (Černý & Ercit, 2005).

Generally, the PC association showing $SiO_2$ dominance with minimal $Fe_2O_3$ and $TiO_2$ validates geochemical analysis results indicating that Akpet quartz has few mineral inclusions and high purity. High PC loadings also reflect that feldspar, mica, and carbonate inclusions contribute $Al_2O_3$, $TiO_2$, MgO, and CaO, reducing quartz purity and reflecting host lithology.

For Betem, the strong REE-Zr-Nb-Y-Hf-Ti association observed in PC1 indicates accessory mineral inclusions such as zircon, monazite, xenotime, and titanite. This shows Betem quartz contains more inclusions and is not fully pure, consistent with a pegmatitic or high-temperature hydrothermal origin. Negative loading of Sb, Bi, and Se indicates late-stage hydrothermal or sulfide-rich phases. PC2 high positive loadings for Rb (0.774), $K_2O$ (0.740), and Cs (0.621) reflect alkali feldspar inclusions or alteration, while negative loadings for Sr (-0.513) and Ca (-0.514) suggest absence or leaching of plagioclase/calcic phases. High loadings of $Fe_2O_3$ (0.476), MnO (0.594), Co (0.519), Cr (0.546), and moderate Ni/Zn loadings indicate Fe-Mn oxides or sulfide inclusions. Positive loadings of Be (0.555), Ga (0.614), Li (0.529), and B (0.532) point to pegmatitic/felsic mineralization, consistent with rare-element pegmatites and potential Li-Be-Ta phases (Černý & Ercit, 2005; London, 2008).

#### *3.4.2.3 Economic appraisal of Akpet and Betem Quartz*

Al and Ti are indicators of quartz quality. Table 4 shows Akpet quartz has lower impurity levels than Betem, placing it in the medium-purity category, with potential for upgrade to high-purity quartz using cost-effective beneficiation. Low Al and Ti concentrations facilitate easier impurity removal. Beneficiation techniques such as acid leaching, thermal treatment, or flotation can reduce impurities further (Lin et al., 2020).

In contrast, high Al and Ti in Betem quartz place it in the low-purity category, requiring extensive and costly processing to achieve high-purity standards. Advanced techniques like high-pressure acid leaching or specialized thermal treatments may improve purity (Xia et al., 2023; Lin et al., 2018). Akpet quartz is suitable for ceramics, glass, and metallurgical-grade silicon production, while Betem quartz is better suited for construction or lower-grade industrial uses unless economically viable purification methods are applied.

In terms of economic viability, Akpet quartz presents a better balance between beneficiation feasibility and industrial applicability, particularly for medium- to high-purity applications. Betem quartz may be limited to low-value applications unless purification costs become justifiable. This study recommends prioritizing development of cost-effective beneficiation techniques for Akpet quartz. For Betem quartz, research into advanced purification methods or alternative uses tolerating higher impurity levels (e.g., construction) is advised.

Beneficiation methods for upgrading Akpet quartz to high-purity include acid leaching (HF, HCl, $H_2SO_4$) to remove Al, Ti, and metallic oxides. The method is cost-effective and scalable but requires proper chemical handling. Alkaline leaching (NaOH) is effective for Al removal with minimal quartz damage. High-

pressure acid leaching achieves higher purity under high pressure and temperature for Al and Ti removal (Xia et al., 2023).

#### *3.4.2.5 Contribution to knowledge and justification for industrial application*

This study bridges the gap between geochemical characterization and industrial applicability of quartz deposits in southeastern Nigeria. Akpet quartz is technically and economically more viable for beneficiation into higher-grade products, while Betem quartz poses challenges for high-purity applications.

The study is justified by the growing global demand for high-purity quartz, especially in semiconductor, photovoltaic, and advanced materials sectors. Nigeria, and West Africa, can contribute to the global supply if resources are properly assessed and developed. Comparing Akpet and Betem establishes economic potential, guiding future beneficiation research, industrial investment, and sustainable resource utilization.

## 4.0 Conclusion

This study conducted a comparative assessment of pegmatite-hosted pegmatite quartz veins in Akpet and Betem, southeastern Nigeria, to evaluate their potential as sources of high-purity quartz (HPQ).

The Akpet quartz is interpreted to have formed under orogenic conditions during the Pan-African orogeny, likely sourced from metamorphic fluids associated with crustal deformation. Its quartz is characterized by low titanium (Ti) and moderate aluminum (Al) contents, indicative of high-pressure, moderate-temperature fluid regimes typical of orogenic systems. Texturally, Akpet quartz displays recrystallized grains and deformation features consistent with vein formation in shear zones.

Conversely, the Betem quartz is genetically linked to a shallow crustal magmatic-hydrothermal system, forming under epithermal conditions (<300°C), with higher Ti and Al concentrations. Its textures—such as colloform banding and vuggy quartz—support formation from dynamic, metal-rich fluids in an open-space environment. This quartz bears geochemical signatures of evolved pegmatitic systems and contains higher levels of incompatible trace elements such as Li, Be, and Rb, which reflect strong magmatic differentiation.

Trace element data and major oxide compositions revealed that Akpet quartz exhibits fewer mineral inclusions and lower concentrations of impurities such as Al, Ti, and Li, aligning it closer to medium-purity quartz (MPQ) standards. In contrast, Betem quartz displayed high impurity levels, with Al and Ti contents exceeding HPQ thresholds, making it less favorable for high-tech applications without extensive beneficiation.

Principal Component Analysis (PCA) and t-tests affirmed the geochemical divergence between the two deposits, with Akpet quartz showing a stronger $SiO_2$ dominance and minimal $Fe_2O_3$ and $TiO_2$ loading—characteristics of purer quartz material. Betem quartz, however, showed enrichment in rare earth and transition elements (Zr, Nb, Y, Ti, etc.), indicative of accessory mineral inclusions and pegmatitic origins.

From an economic perspective, Akpet quartz shows better potential for beneficiation into HPQ, given its relatively low impurity levels and favorable geochemical characteristics. Acid leaching, alkaline treatment, and thermal processes can improve its purity cost-effectively. Betem quartz, by contrast, would require advanced purification techniques, which may not be economically viable for HPQ production. It is more suitable for low- to medium-grade applications such as construction materials unless high-value by-products (e.g., rare metals) are targeted.

Despite both locations falling short of global HPQ standards in their raw state, Akpet quartz shows significant promise as a feedstock for high-purity applications after processing, while Betem quartz may be more viable for industrial or construction-grade applications or as a source of rare metal elements. Hence, the findings provide a scientific basis for the exploration and development of granite-hosted quartz veins in southeastern Nigeria and offer guidance for the targeted production of high-purity quartz in similar geological terrains.

**Acknowledgement**

The authors would like to acknowledge all the authors for their contribution to ensuring a successful completion of this research work. The authors also acknowledge Müller *et al.* (2010,

and 2012 a & b), Götze (2009, 2012; Götze *et al.,* 2004), and Akweteri, A. A., & Nwachukwu, M. A. (2010) whose works were instrumental in this research.

## 5.0 References


Ajibade, A. C., & Wright, J. B. (1981). Structural relationship in the schist belts of Nigeria. In *Precambrian Geology of Nigeria*, 57–69. Geological Survey of Nigeria.

Akweteri, A. A., & Nwachukwu, M. A. (2010). Geochemical characterization of quartz deposits in Anambra Basin. *Nigerian Journal of Mining and Geology*, *46*(2), 85–96.

Akweteri, A. A., & Nwachukwu, M. A. (2010). Geochemical characteristics of quartz in the Anambra Basin and its implications for industrial application. *Nigerian Journal of Geosciences*, 6(1), 45–54.

Černý, P., & Ercit, T. S. (2005). The classification of granitic pegmatites revisited. *Canadian Mineralogist*, 43(6), https://doi.org/10.2113/gscanmin.43.6.2005

Edet, A., Ukpong, A., Ekwere, A., Wiche, O., Nganje, T., Adamu, C., & Kudamnya, E. (2025). Assessment of surface water and groundwater quality and their associated human health risks around dumpsites, Cross River State, Southern Nigeria. *Environmental Earth Sciences*, 84(9), 234.

Egesi, N., & Ukaegbu, V. U. (2010). Trace and Rare Earth Element Geochemical Fingerprints on the Petrogenesis and Geotectonics of the Enderbite-Adamellite-Granite Complex in Parts of Bansara (Sheet 304 NE and SE), Southeastern Nigeria. *IUP Journal of Earth Sciences*, 4(2).

Ekwueme, B. N. (1990). Rb-Sr ages and petrologic features of Precambrian rocks from the Oban Massif, southeastern Nigeria. *Precambrian Research*, 47(3-4), 271-286.

Ekwueme, B. N., & Matheis, G. (1995). Geochemistry and economic value of pegmatites in the Pre-cambrian basement of Southeast Nigeria. *IBH Publishing Co., New Delhi, India*, 375-392.

Elueze, A. A. (1981). Petrographic and chemical characteristics of chromite-bearing ultramafic rocks in Nigeria. *Journal of Mining and Geology*, 18(1), 20–30.

Garba, I. (2003). Geochemical discrimination of newly discovered rare-metal bearing and barren pegmatites in the Pan-African (600±150 Ma) basement of northern Nigeria. *Applied Earth Science*, 112(3), 287-292.

Geological interpretation and technical application. *Mineralogical Magazine*, 73(4), 645–671. https://doi.org/10.1180/minmag.2009.073.4.645

Götze, J., Nasdala, L., & Wenzel, M. (2004). Trace element incorporation into quartz: A combined SIMS, cathodoluminescence and TEM study. *Contributions to Mineralogy and Petrology*, 147(4), 443–456. https://doi.org/10.1007/s00410-004-0563-0

Götze, J. (2009). Chemistry, textures and physical properties of quartz—Geological interpretation and technical application. *Mineralogical Magazine*, 73(4), 645-671.

Götze, J. (2012). Application of cathodoluminescence (CL) microscopy and spectroscopy in geosciences. *Micron*, 43(5), 546–562.

Harben, P.W. (2002): The industrial mineral handy book—a guide to markets, specifications and prices, 4th edn. Industrial Mineral Information. Worcester Park, 412.

Haus, R. (2005): High demands on high purity. Industrial Minerals 10: 62–67.

Haus, R., Prinz, S., Priess, C. (2012): Assessment of High Purity Quartz Resources, *J. Götze and R. Möckel (eds.), Quartz: Deposits, Mineralogy and Analytics, Springer Geology, Springer-Verlag Berlin Heidelberg*, 29-51.

http://www.ngu.no/en-gb/hm/Resources/industrimineraler/Kvarts-og-kvartsitt/High-purity-quartz/. Accessed 26 December, 2013.

IOTA (2013): IOTA high purity quartz. http://www.IOTAquartz.com/techIOTA4data.html Accessed 20 December, 2013

Kerrich, R., Fyfe, W. S., & Maclennan, S. (1980). Chemistry of Archean volcanic rocks in the Abitibi greenstone belt: Implications for hydrothermal activity and

crustal evolution. *Geochimica et Cosmochimica Acta*, 44(4), 475–484. https://doi.org/10.1016/0016-7037(80)90007-7

Lehmann, E. L., & Romano, J. P. (2005). Testing statistical hypotheses. New York, NY: Springer New York.

Lin, Y., Liu, D., He, Y., & Li, W. (2018). Influence of impurities on high-purity quartz processing and application. *Journal of Non-Crystalline Solids, 492*, 49–56. https://doi.org/10.1016/j.jnoncrysol.2018.03.035

Lin, Y., Liu, D., Zhang, Y., & Li, W. (2020). A review of purification technology of quartz for high-purity applications. *Ceramics International*, 46(6), 7417–7428. https://doi.org/10.1016/j.ceramint.2019.11.256

London, D. (2008). *Pegmatites*. Mineralogical Association of Canada Short Course Series Vol. 10. Québec: MAC.

Meinhold, G. (2010). Rutile and its applications in earth sciences. *Earth-Science Reviews*, 102(1-2), 1-28.

Müller, A., Herrington, R., Armstrong, R., Seltmann, R., Kirwin, D.J., Stenina, N.G., Kronz, A. (2010): Trace elements and cathodoluminescence of quartz in stockwork veins of Mongolian porphyry-style deposits. Mineralium Deposita, 45, 707–727.

Müller, A., Wirth, R., & Höhndorf, A. (2012). Microstructural and geochemical features of quartz from orogenic gold deposits. *European Journal of Mineralogy*, 24(4), 655–667. https://doi.org/10.1127/0935-1221/2012/0024-2207

Müller, A., Wirth, R., & Höhndorf, A. (2012). Quartz recrystallization and element mobility in Norway's Svecofennian Belt. *European Journal of Mineralogy*, *24*(4), 655–667.

Norwegian Crystallites AS (2013): Norwegian Crystallites AS-products-crystal quartz analyses. Accessed 20th November 2013. http://www.norcryst.no.

Obaje, N. G. (2009). The Basement Complex. In N. G. Obaje, Geology and Mineral Resources of Nigeria. *Springer Berlin Heidelberg*, 120, 13–30 https://doi.org/10.1007/978-3-540-92685-6_2

Obaje, N.G. (2009). *Geology and Mineral Resources of Nigeria*. Springer.

Omang, B. O., Arikpo, T. O., Abam, E. G. W., Kave, G. T., Asinya, A. E., & Onasanwo, A. A. (2024). The Geochemistry and Petrogenesis of the Iron-Bearing Sediments of Mfamosing, Southeastern (SE), Nigeria: Evidence from Major Oxides and Its Implication for Industrial Utilization. *Communication in Physical Sciences*, 11(4).

Omang, B. O., Ngwu, U. N., Arikpo, T. O., Chukwura-Osoagba, U., Kave, G. T., & Ephriam, B. E. (2025). A comparative assessment of Lepidolite-bearing pegmatites from Akpet and Betem areas, Southeastern Nigeria: insights from their geochemical signatures and economic potential. *Applied Sciences, Computing, and Energy*, 3(1), 41-65.

Oyinloye, A. O. (2011). Geochemistry and petrogenesis of pegmatites and associated rocks in southwestern Nigeria: Implications for rare-element mineralization. *Journal of Mining and Geology*, 47(1), 15–28.

Petters, S. W. (Ed.). (1991). Chapter 6 Late Proterozoic-Early Paleozoic Pan-African Mobile Belts. In Regional Geology of Africa. *Springer-Verlag*, 40, 254–420. https://doi.org/10.1007/BFb0020583

Rahaman, M. A. (1988). Recent advances in the study of the basement complex of Nigeria. *Precambrian Geology of Nigeria*, 11–43. Geological Survey of Nigeria.

Rusk, B. G., Lowers, H. A., & Reed, M. H. (2008). Trace elements in hydrothermal quartz: Relationships to cathodoluminescent textures and insights into vein formation. *Geology*, 36(7), 547-550.

Rusk, B. (2012). Cathodoluminescent textures and trace elements in hydrothermal quartz. In *Quartz: Deposits, mineralogy and analytics*. *Berlin, Heidelberg: Springer Berlin Heidelberg*, 307-329.

Thomas, R., Förster, H. J., & Heinrich, W. (2011). The behaviour of trace elements in quartz from granite pegmatites. *American Mineralogist*, 96(10), 1445–1463. https://doi.org/10.2138/am.2011.3751

Ukaegbu, V. U., & Ekwueme, B. N. (2006). Petrogenesis and geotectonic setting of the Pan-African basement rocks in Bamenda Massif, Obudu Plateau, southeastern Nigeria: Evidence from trace element geochemistry. *Chinese Journal of Geochemistry*, 25(2), 122–131. https://doi.org/10.1007/BF02872171

Wark, D. A., & Watson, E. B. (2006). TitaniQ: A titanium-in-quartz geothermometer. *Contributions to Mineralogy and Petrology*, 152(6), 743–754. https://doi.org/10.1007/s00410-006-0132-1

Xia, X., Zuo, Y., Liu, H., & Li, R. (2023). Advances in impurity removal from quartz: Industrial beneficiation and purification methods. *Applied Geochemistry*, 152, 105–582. https://doi.org/10.1016/j.apgeochem.2023.105582

Xia, Y., Zhang, Z., & Li, W. (2023). SEM-EDS characterization of quartz in Precambrian rocks of the Canadian Shield. *Geochemistry: Exploration, Environment, Analysis*, 23(1), 79–90.

Yardley, B. W. D. (1989). *An Introduction to Metamorphic Petrology*. Longman Earth Science Series.

**Declaration**

**Competing Statement: Financial Interests Statement:**
There are no competing financial interests in this research work.

**Ethical considerations**
Not applicable

**Data availability**
The microcontroller source code and any other information can be obtained from the corresponding author via email.

**Funding sources**
The authors declared no source of funding

## Authors' Contribution

First Author: Project concepualization, design, and supervision. Second Author: Writing, results extraction. Third Author: Analysis, manuscript first draft. Fourth and Fifth Authors: Manuscript revision, review, and proofreading.